Mutation Research 692 (2010) 12–18

Contents lists available at ScienceDirect

Mutation Research/Fundamental and Molecular Mechanisms of Mutagenesis

journal homepage: www.elsevier.com/locate/molmut
Community address: www.elsevier.com/locate/mutres

Live cell imaging of micronucleus formation and development

Manabu Yasui[a,*], Naoki Koyama[b], Tomoko Koizumi[a], Kaori Senda-Murata[c], Yoshio Takashima[d], Makoto Hayashi[e], Kenji Sugimoto[c], Masamitsu Honma[a]

[a] Division of Genetics and Mutagenesis, National Institute of Health Sciences, 1-18-1 Kamiyoga, Setagaya, Tokyo 158-8501, Japan
[b] Graduate School of Nutrition and Environmental Sciences, University of Shizuoka, 52-1 Yada, Suruga-ku, Shizuoka 422-8526, Japan
[c] Division of Biosciences and Informatics, Osaka Prefecture University, 1-1 Gakuen-cho, Nakaku, Sakai, Osaka 599-8531, Japan
[d] Research Center for Radiation Emergency Medicine, National Institute of Radiological Sciences, 4-9-1 Anagawa, Inage, Chiba 263-8555, Japan
[e] Biosafety Research Center, Foods, Drugs and Pesticides, 582-2 Shioshinden, Iwata-shi, Shizuoka 437-1213, Japan

ARTICLE INFO

Article history:
Received 19 April 2010
Received in revised form 26 July 2010
Accepted 28 July 2010
Available online 5 August 2010

Keywords:
Micronucleus test
Micronuclei
Chromosome aberration
Aneuploid
M-phase

ABSTRACT

The micronucleus (MN) test is widely used to biomonitor humans exposed to clastogens and aneugens, but little is known about MN development. Here we used confocal time-lapse imaging and a fluorescent human lymphoblastoid cell line (T105GTCH), in which histone H3 and α-tubulin stained differentially, to record the emergence and behavior of micronuclei (MNi) in cells exposed to MN-inducing agents. In mitomycin C (MMC)-treated cells, MNi originated in early anaphase from lagging chromosome fragments just after chromosome segregation. In γ-ray-treated cells showing multipolar cell division, MN originated in late anaphase from lagging chromosome fragments generated by the abnormal cell division associated with supernumerary centrosomes. In vincristine(VC)-treated cells, MN formation was similar to that in MMC-treated cells, but MNi were also derived from whole chromosomes that did not align properly on the metaphase plate. Thus, the MN formation process induced by MMC, γ-rays, and VC, were strikingly different, suggesting that different mechanisms were involved. MN stability, however, was similar regardless of the treatment and unrelated to MN formation mechanisms. MNi were stable in daughter cells, and MN-harboring cells tended to die during cell cycle progression with greater frequency than cells without MN. Because of their persistence, MN may have significant impact on cells, causing genomic instability and abnormally transcribed genes.

© 2010 Elsevier B.V. All rights reserved.

1. Introduction

The micronucleus (MN) test is widely used to biomonitor humans exposed to clastogens and aneugens [1–4] and has recently become a useful tool for predicting cancer risk [5–8]. Micronuclei (MNi), which consist of chromatin (chromosomes and chromosome fragments), are formed dose-dependently in parallel with increasing concentrations of clastogens and aneugens both *in vitro* and *in vivo* [9–11].

The two basic mechanisms that give rise to MNi during M-phase are chromosome breakage and spindle apparatus defects (for review, see [12]). MNi originate as lagging acentric chromosome fragments and/or as whole chromosomes that fail to bind to the mitotic spindle during cell division. In addition, some MNi are formed from fragments induced by broken anaphase bridges [13,14]. Such mechanisms, however, are speculations based on the analysis of fixed cells. Direct observations of the active process are few [15–17]. Moreover, the fate of MNi after they first appear at M-phase remains uncertain. If they persist in the cytoplasm during cell cycle progression [16], they might have significant impact. Genes on MN, for example, may be transcribed extrachromosomally [18–20] and influence the cell's phenotype.

Since MN formation is dynamic and rapid (lasting a few minutes) and may occur unseen behind a main nucleus, live-cell analysis at long intervals without confocal recording is inadequate to capture the event and also cannot distinguish whether a MN originates from a chromosome fragment or a whole chromosome. Here we used multi-fluorescent cells and three-dimensional, high-resolution imaging over short intervals to accurately record when, where, and how MN originates and concludes in live cells. We constructed for the study dual-color fluorescent T105GTCH cells in which histone H3 and α-tubulin were differentially expressed as fusion to monomeric Cherry (mCherry) and enhanced green fluorescent protein (EGFP), respectively. Using those cells and a high-resolution imaging system, we investigated the life cycle of MN induced by exposure to mitomycin C (MMC; a crosslinking agent), γ-rays (a strand-breaking agent), and vincristine (VC; a spindle poison).

Abbreviations: MN, micronucleus; MNi, micronuclei; MMC, mitomycin C; VC, vincristine; GFP, green fluorescent protein; CFP, cyan fluorescent protein.

* Corresponding author. Tel.: +81 3 3700 1141x434; fax: +81 3 3700 2348.
E-mail address: m-yasui@nihs.go.jp (M. Yasui).

0027-5107/$ – see front matter © 2010 Elsevier B.V. All rights reserved.
doi:10.1016/j.mrfmmm.2010.07.009

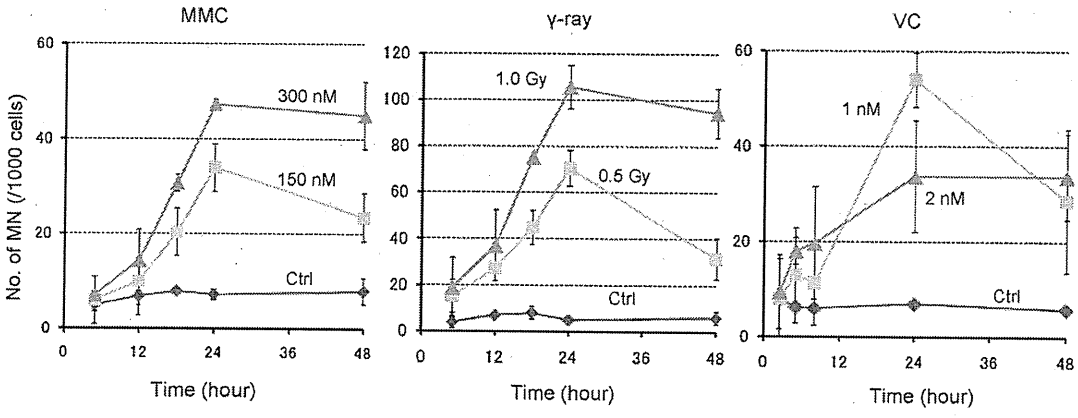

Fig. 1. *MN induction by MMC, γ-rays, and VC*: MMC, γ-rays, and VC induced MNi in T105GTCH cells dose-dependently and peaked 24 h after treatment. Control cell MN frequencies were ~5 MNi per 1000 cells.

2. Materials and methods

2.1. General

We obtained MMC from Kyowa Hakko Bio Co., Ltd. (Tokyo) and VC from Wako Pure Chemical Industries, Ltd. (Tokyo) and dissolved them in phosphate-buffered saline (Takara Bio Inc., Shiga, Japan) just before use. We delivered γ-ray irradiation with a Gammacell 40 Exactor (MDS Nordion, Canada). We purchased RPMI1640 medium, penicillin, and streptomycin from Invitrogen Corp. (USA), horse serum from JRH Biosciences (USA), sodium pyruvate from Sigma–Aldrich Corp. (USA), Dulbecco's modified Eagle's medium from Nacalai Tesque Inc. (Kyoto, Japan), and fetal calf serum from MP Biomedicals Inc. (USA).

2.2. Cell culture

We grew T105GTCH cells (derived originally from human lymphoblastoid cell line TK6 [21,22]) in RPMI1640 medium supplemented with 10% heat-inactivated horse serum, 200 μg/ml sodium pyruvate, 100 U/ml penicillin, and 100 μg/ml streptomycin and maintained them at 10^5–10^6 cells/ml at 37 °C in a 5% CO_2 atmosphere with 100% humidity. We maintained fluorescent MDA-435 cells (constructed by Sugimoto [23,24]) in Dulbecco's modified Eagle's medium containing 10–15% fetal calf serum at 37 °C in a 5% CO_2 atmosphere with 100% humidity.

2.3. Preparation of pEGFP-Tub and pmCherry-H3 plasmid

We obtained pEGFP-Tub containing human α-tubulin cDNA from BD Biosciences, Clontech. We constructed pmCherry-H3 by replacing the EGFP cDNA of pEGFP-H3 [23] with mCherry cDNA that we amplified by PCR using pRSET-B mCherry [25] (provided by Prof. Roger Y. Tsien, University of California, San Diego) as a template.

2.4. Construction of dual-color fluorescent cell line T105GTCH

pEGFP-Tub and pmCherry-H3 expression vectors, 20 μg each, were mixed with 5×10^6 TK6 cells in 100 μl Nucleofector Solution V, containing 18% Supplement 1 (Amaxa Inc., USA) and tranfected into the cells with Amaxa Nucleofector (Amaxa Inc., USA) at a setting of A-30. The vector-integrated cells were selected in the presence of G418 (750 μg/ml) and collected 10 days later. We selected single colonies of stably transfected cells with the aid of a fluorescent microscope and cultured them for 2 more weeks.

2.5. MN test

We carried out the MN test on 5×10^5 T105GTCH cells at 0, 5, 12, 18, 24, and 48 h after treatment with MMC (150 or 300 nM for 4 h followed by a PBS rinse), γ-rays (0.5 or 1 Gy), or VC (1 and 2 nM). We suspended approximately 10^6 treated cells in hypotonic KCl solution (75 mM), incubated them for 10 min at room temperature, fixed them twice with ice-cold glacial acetic acid in methanol (1:3), and resuspended them in methanol containing 1% acetic acid. We placed a drop of the suspension on a clean glass slide and allowed it to air-dry. We then stained the cells with 40 μg/ml acridine orange solution and observed them immediately with the aid of a fluorescence microscope (Olympus Corp., Tokyo). We examined at least 1000 intact interphase cells for each treatment and scored the cells containing MNi, which we defined by size as equal to or less than one-third the size of the main nucleus.

2.6. Live cell imaging for capturing MN formation

We cultured 5×10^5 T105GTCH cells in 2 ml RPMI1640 medium with a 35 mm BAM-coat dish (NOF Corp., Tokyo), which retained the cells for ~4 h on the surface, in a humid chamber set at 37 °C and 5% CO_2 on the stage of a fluorescent microscope in FV1000 system (Olympus Corp., Tokyo) equipped with

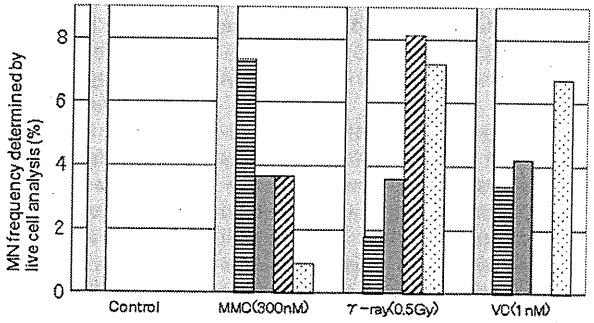

	Control	MMC(300nM)	γ-ray(0.5Gy)	VC(1 nM)
Normal cell division	100.0	84.4	80.2	85.7
MN formation during bipolar division	0.0	7.3	1.8	3.4
Multipolar cell division	0.0	3.7	3.6	4.2
MN formation during multipolar division	0.0	3.7	8.1	0.0
Cell death	0.0	0.9	7.2	6.7

Fig. 2. *MN formation in T105GTCH cells analyzed by live cell imaging*: From 22 to 25 h we recorded moving images of 109 cell divisions following treatment with MMC (300 nM), 111 following irradiation with γ-rays (0.5 Gy), and 119 following treatment with VC (1 nM). MN frequencies (%) are presented by category. All control cells divided normally with no evidence of MN formation.

computer-controlled confocal and multi-stage functions. We used multi-Ar and He–Ne G lasers and 60× (1.20 NA) objective. We captured a time-lapse image every 2–3 min (z-series of 11–16 images with an interval of 1.0–2.0 μm) and reconstructed by Volocity software (Improvision Inc., USA), documenting cell division from 22 to 25 h after treatment with 300 nM MMC (109 cell divisions), 0.5 Gy γ-ray irradiation (111 cell divisions), or 1 nM VC (119 cell divisions). MN in live cell imaging was defined as a whole chromosome or chromosome fragment which is physically distinct from the main group of chromosomes. We examined at least 100 mitotic cells for each treatment and scored cell divisions that gave rise to MN, which we defined by size as equal to or less than one-third the size of the main nucleus. We distinguished between chromosomes and chromosome fragments by using criteria that a metacentric or submetacentric chromosome had two short and long arms (see Fig. 4C), but not a chromosome fragment.

2.7. Statistical analysis

MN frequencies between non-treated and treated cells were statistically analyzed by Fisher's exact test. The concentration–response relationship was evaluated by the Cochran–Armitage trend test [26].

2.8. Long-term live-cell analysis

To investigate the behavior of chromosome-originating MNi up to and through the next cell division after M-phase, we recorded the behavior of MN-bearing MDA-435 cells in which chromatin was visualized with cyan fluorescent proteins (CFP). We exposed cells to MMC (300 nM), incubated them for 24 h, and washed with PBS. We maintained the cells under minimally toxic conditions by using mild laser excitation output (~50% of the visualized control cells divided normally after 24 h) and carried out time-lapse recording at 10–20 min intervals for 24–60 h (z-series of 11–13 images with an interval of 2.0 μm).

3. Results and discussion

3.1. Toxicity of staining system

We isolated the dual-fluorescent T105GTCH clones stably showing red nuclei and green tubulin with the aid of a fluorescent microscope. The growth rate and spontaneous MN frequency for T105GTCH cells were almost the same as those reported for TK6 cells [27,28], indicating that the EGFP and mCherry fluorescent proteins were not cytotoxic.

3.2. Induced MN frequencies

Fig. 1 shows the MN frequencies induced by MMC, γ-rays, and VC over time. The spontaneous MN frequency was ~5/1000 cells (0.5%). MMC, γ-rays, and VC increased the frequencies dose-dependently, peaking at 24 h. The MN frequencies induced by 300 nM MMC, 0.5 Gy γ-ray irradiation, and 1 nM VC were similar (~5%) at 24 h, the time we started the live-cell imaging analysis. At 24 h, the growth rate of cells exposed to each of the MN-inducing agents was only ~20% lower than the growth rate of control cells.

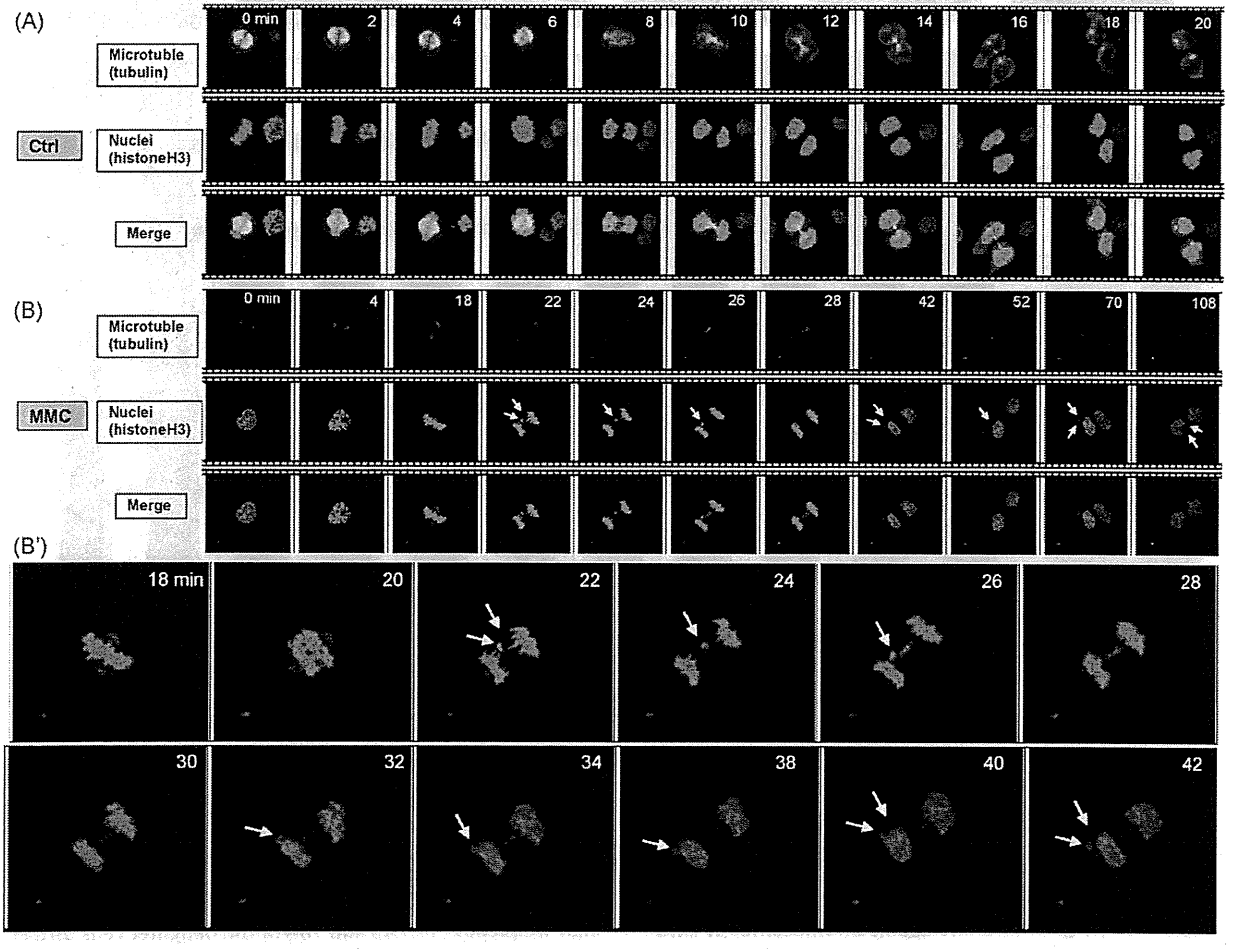

Fig. 3. *Confocal live cell image analysis of cells treated with MMC, γ-rays, and VC*: (A) Normal bipolar cell division (control); no MNi were observed. (B) Normal bipolar cell division in cells treated with MMC (300 nM). Chromosome fragment becoming MNi formed at 22 min, at early anaphase, and remained for 86 min (until the time-lapse recording was over). This sample corresponds to the ID number 4 in Table 1. (C) Multipolar division in cells treated with γ-rays (0.5 Gy). MNi formed at ~122 min, in late anaphase, and remained for 78 min (sample number 21 in Table 1). (D) Normal bipolar division in cells treated with VC (1 nM). MN formed at 22 min, at early anaphase, and repeatedly attached to a daughter nucleus and detached from it (sample number 24 in Table 1).

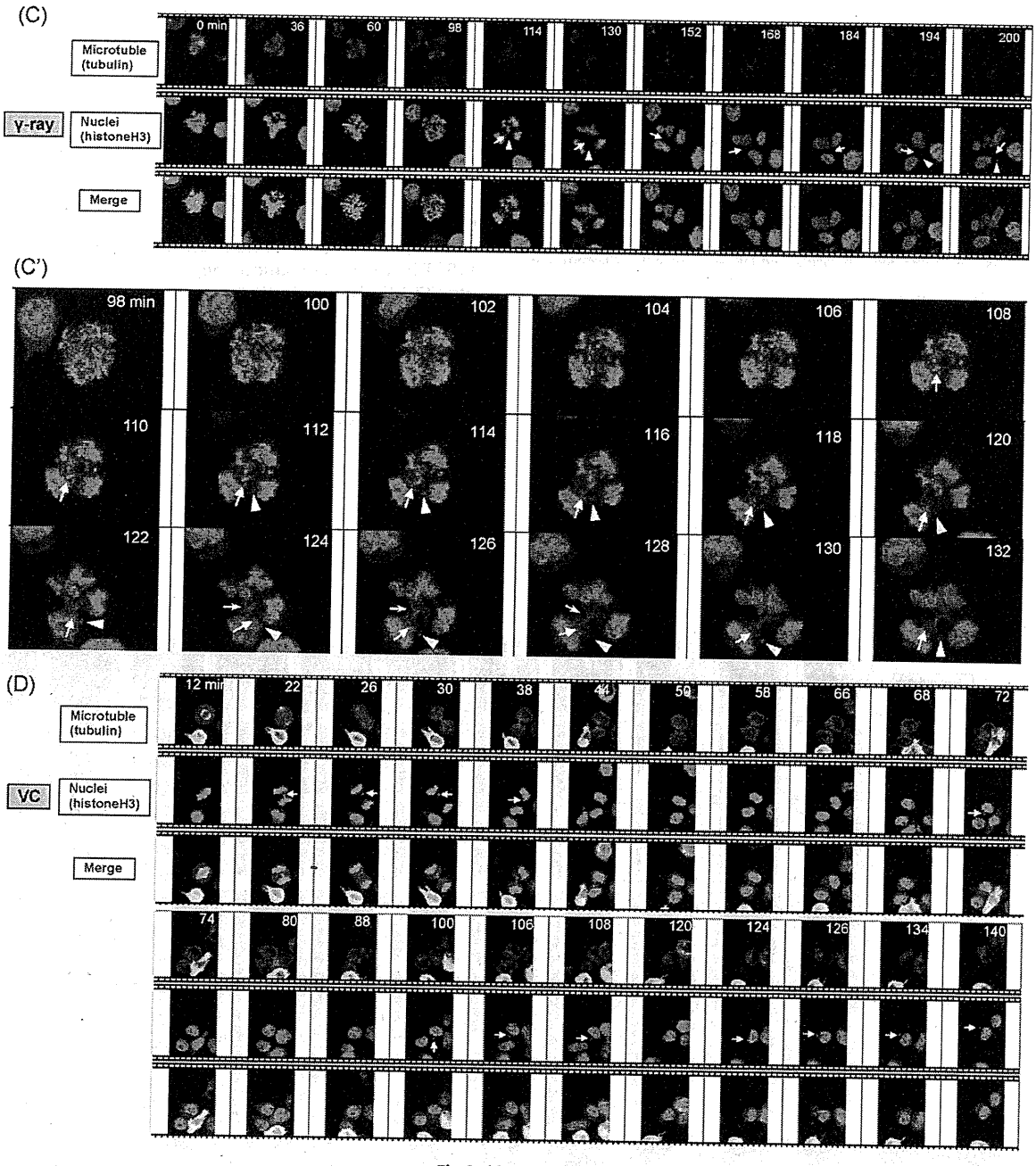

Fig. 3. (*Continued*)

Following exposure to 1 nM VC, ~50% of cells passed the mitotic checkpoint and were used in the live-cell analysis.

3.3. MN emergence captured by confocal time-lapse microscopy

We found at least one MN during bipolar or multipolar mitosis in 12 (~11%) MMC-treated cells, 11 (~10%) γ-ray irradiated cells, and 4 (~3%) VC-treated cells. Fig. 2 shows the categories of cell division that led to MN formation and mitotic catastrophe. Mitotic catastrophe was defined as cell death during M-phase (from prophase to telophase). All MN originated from lagging chromosomes or chromatid fragments and whole chromosomes in this study.

Confocal time-lapse microscopy of control cells recorded normal division with no MN formation evident (Figs. 2 and 3A). Fig. 3B shows the time course of typical MN formation in MMC-treated cells. The MNi originated from two lagging chromosome fragments just after chromosome segregation at early anaphase and immediately became spherical, resulting in the formation of small and large MNi of appropriate thickness for the size of the fragment (arrows in Fig. 3B and B′). Subsequently, the MNi collided with the main nucleus, disappeared from the view (26–30 min), and came out from it at 32 min as shown in Fig. 3B′. The two MNi sometimes came into contact but were independent and did not condense into a single MN by the end of the time-lapse recording (108 min).

Following γ-ray irradiation, multipolar division occurred with high-frequency (11.7%), and 70% of the daughter cells formed MN during divisions that involved 3 or 4 spindle poles (Figs. 2 and 3C). Our finding that γ-ray irradiation increases the abnormal replication of supernumerary centrosomes is in agreement with a report by Sato and colleagues [29]. MN induction involving multipo-

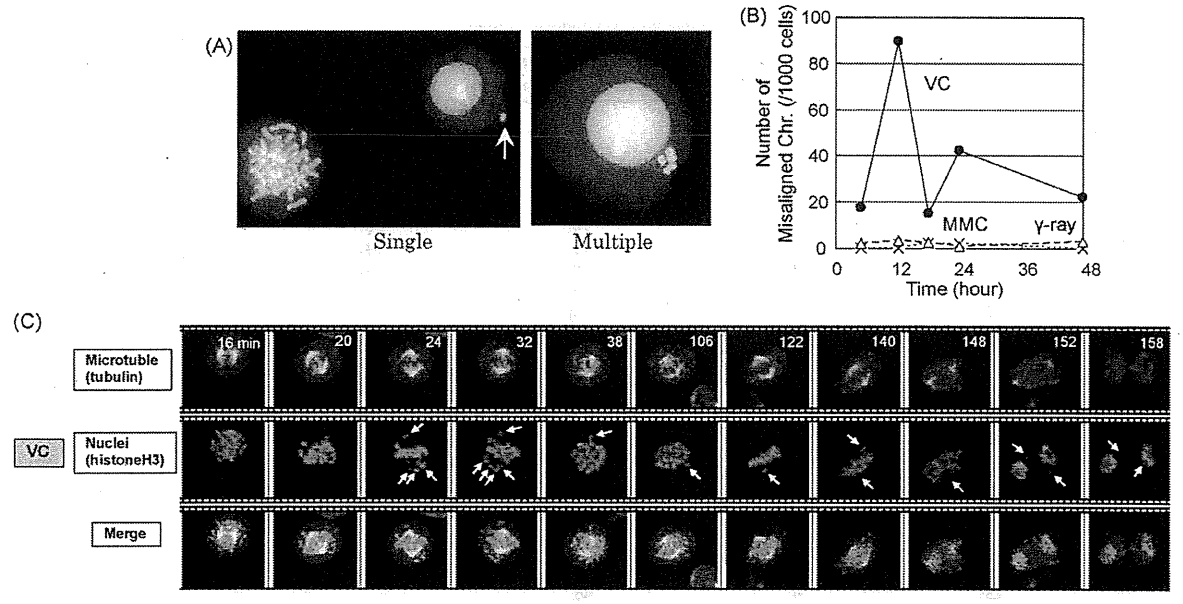

Fig. 4. *Metaphase misalignment in VC-treated cells*: (A) VC-treated cells showing misaligned chromosome, single (left panel) and multiple (right panel), in MN test. (B) The frequency of misaligned chromosomes peaked at 12 h in only VC-treated cells. (C) Misaligned chromosomes were captured at 6–9 h after VC treatment and promoted MN formation and aneuploid. Metacentric and submetacentric chromosomes had two short and long arms and were structurally different from a chromosome fragment.

lar mitosis originated mainly from broken chromosomes at late anaphase, and the MNi were not spherical, showing that MNi induced by γ-rays formed differently from those induced by MMC. In normal cell division, the two sets of chromatid were pulled toward two spindle poles for equal distribution into daughter cells (Fig. 3A) [30]. In multipolar mitosis, however, chromosomes were pulled toward to 3 or 4 sides of the multipolar spindle and simultaneously broken off into small pieces (100–108 min) at early anaphase, resulting in the formation of broken chromosome specks (arrows in Fig. 3C′). We here define that a chromosome speck is generated by fatal breakage of chromosome or chromosome fragment in anaphase and is not spherical. Fragments and specks mostly entered the main nucleus (108–118 min) but some specks did not re-enter the main nucleus. At the beginning of telophase, the more lagging fragments (Fig. 3C and C′, arrowheads) also could not enter the main nucleus in daughter cells. Meanwhile, a fraction of lagging specks disappeared in mid-body when the cells split at telophase (124–128 min), indicating DNA loss (Fig. 3C′, yellow arrows).

Following VC treatment, spherical MNi (3.4%) formed at anaphase similar to the way they formed following MMC treatment (Fig. 3B and D). Cell death (6.7%) by mitotic catastrophe also occurred due to detrimental karyotypic changes induced by VC. Another factor causing the MN frequency to increase was intact chromosomes that did not align on the metaphase plate (Fig. 4C, arrows), which were also detectable in the MN test (Fig. 4A). The frequency of misaligned chromosomes peaked at 12 h (Fig. 4B). We captured some misaligned chromosomes becoming MNi, but the frequency was low because of a p53-dependent check point [30,31] in the T105GTCH cells during meta-anaphase (Fig. 4C). Thus, the initiation time for MN formation induced by VC began at metaphase.

3.4. MN formation mechanisms varied with the MN-inducing agent

The spherical MN had an appropriate thickness for the size of the whole chromosome (Fig. 4C) and chromosome fragment (Fig. 3B and D). It was induced by MMC and VC treatment in this study. The aspherical MN originated from chromosome specks generated by fatal breakage of chromosome or chromosome fragment induced by γ-rays in this paper. The density (DNA content) of aspherical MN would be lower than that of spherical one because the chromosome specks were formed by the complex fragmentation and expansion of small chromosome fragments which pulled toward to 3 or 4 sides of multipolar spindle during cell division, resulting in the formation of low density MN (Fig. 3C).

MMC, a potent DNA crosslinking agent [32], induces fragmented chromosomes. We found that the frequency of MN originating from lagging chromosome fragments at anaphase during normal mitosis was induced by the 3 agents in the order MMC > VC > γ-rays (Fig. 2). Following VC treatment, and only VC treatment (Fig. 4B), we observed MNi formed by intact chromosomes that did not align at the metaphase plate, but we did not detect any during multipolar cell division (Fig. 2). That is because VC binds to tubulin dimers, inhibiting assembly of microtubule structures, but it is not a DNA damaging agent (VC is Ames-test negative) and so does not promote chromosome fragments. In multipolar division, in contrast, γ-rays induced more MNi than MMC (Fig. 2). That can be explained by the fact that γ-rays can simultaneously induce DNA strand breaks (forming chromosome fragments) and abnormal amplification of centrosomes (increasing the frequency of aberrant mitoses and chromosome segregation errors). Thus, the typical events of MN formation induced by MMC, γ-rays, and VC were strikingly different, suggesting that different mechanisms were involved.

3.5. Behavior and stability of MNi after cell division

MNi first appeared during M-phase, and we tracked them and studied their behavior and stability during G1-phase with T105GTCH cells. The MNi were dynamic and sometimes moved behind the nucleus, and they remained stable in the cytoplasm of daughter cells for a few hours (until the time-lapse recording was over) as shown by the column of Stability of MN in Table 1. That observation was consistent with a previous report using the UPCI SCC oral squamous cell carcinoma cell line [16]. We also found that MN stability was similar and unrelated to the toxic action of MN-inducing MMC, γ-rays, and VC (Table 1). Interestingly, only in bipolar mitoses, MNi repeatedly attached to a daughter nucleus and detached from it at a later time (Fig. 3D, corresponding to the

Table 1
MN formation and stability observed in T105GTCH cells following treatment with MN-inducing agents.

MN-inducing agent	Sample ID number	Number of mitotic spindles	Time of MN formation (min)	Time when MNi interacted with main nucleus (min)[a]	Stability of MN (min)
MMC	1	2	14	*22*-**26**-*28*	–
	2	2	14	*16*-**24**-*26*-**30**-*34*	–
	3	2	6	*20*-**22**-*38*-**44**	–
	4	2	22	*28*-**32**	–
	5	2	20	*42*	22
	6	2	10	*20*	10
	7	2	12	*54*	42
	8	2	16	*34*	18
	9	3	6	–	16
	10	3	6	–	20
	11	4	28	–	20
	12	3	6	–	50
γ-Rays	13	2	20	*62*	42
	14	2	90	*168*	78
	15	4	48	*116*	68
	16	3	40	–	20
	17	3	36	–	24
	18	3	22	–	40
	19	3	90	–	40
	20	3	20	–	42
	21	4	122	–	78
	22	4	30	–	140
	23	4	48	–	250
VC	24	2	22	*38*-**72**-*74*-**92**-*118*-**124**	–
	25	2	156	*182*	26
	26	2	68	*96*	28
	27	2	40	–	110

[a] Italic and bold types indicate when MN attached to and detached from the main nucleus, respectively.

sample number 24 in Table 1). The relationship between MN interaction with the main nucleus and the polar number in cell division, however, is unclear.

In long-term live-cell analysis performed by under mild laser excitation output, approximately 50% of non-treated MDA-435 control cells normally divided after 24 h (Animation 1). Animation 2 shows typical MN fates in MMC-treated MDA-435 cells we observed with long-term live-cell analysis. As shown in Fig. 5, only 5 (5%) of the 98 interphase cells harboring MMC-induced MNi proceeded to M-phase (Fig. 5c), and 4 cells of them underwent mitotic catastrophe (d). MNi in 68 (69%) of the cells persisted in the cytoplasm for the full observation time (a). Thus, MN stability was similar to that obtained from the above experiment with T105GTCH cells. Besides, cell cycle progression was delayed in MN-harboring cells, and their cell death was approximately 2.5-fold higher than that of cells without MN because of their genomic instability increased by MN and the laser excitation effect (b). It is possible that all MN-bearing cells eventually die (Fig. 5(b) and (d)). Thus, MN may have significant impact on cells because of their persistence. MN in 1 (1%) of the cells disappeared from the cytoplasm, where it may have been degraded. We also observed blebbing MNi in 2% of the cells. In a previous report [33], an elimination mechanism of MN from the cell was suggested, but we did not observe that in this study.

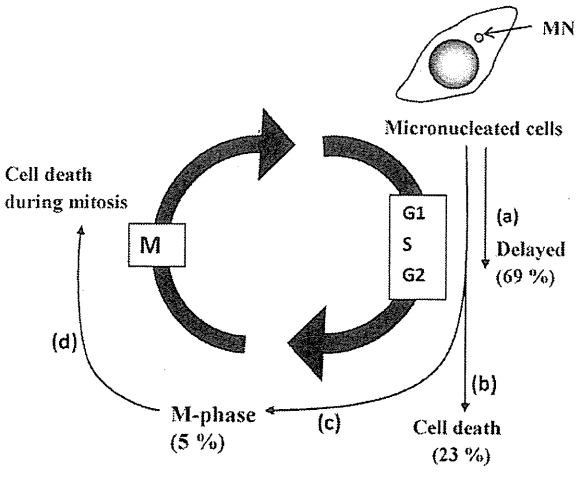

Fig. 5. Diagram of fates of micronucleated cells based on long-term live-cell imaging of fluorescent MDA-435 cells exposed to MMC (300 nM).

In conclusion, in this confocal microscopic study of live T105GTCH cells exposed to three kinds of MN-inducing agents, we found that MNi can be generated by strikingly different mechanisms. After MNi emerge, however, their stabilities are similar and unrelated to MN formation mechanisms. Long-term live-cell analysis of chromatin-visualized MDA-435 cells suggested that MN-harboring cells tended to die during cell cycle progression with greater frequency than cells without MN. Because of their persistence, MN may have significant impact on cells, causing genomic instability and abnormally transcribed genes.

Conflict of interest statement

The authors declare that there are no conflicts of interest.

Acknowledgment

We are grateful to Dr. Roger Y. Tsien for providing pRSET-B mCherry plasmid. We thank Ms H. Sakamoto, M. Sakuraba, and A. Ukai for experimental assistance. This study was supported by Grant-in-Aid for JSPS Fellow (20/08797) and Health and Labor Sciences Research Grants (H21-chemical-general-008) in Japan (to M.H.). This work was also partially supported by Grants-in-aid for Scientific Research 19710059 from the Ministry of Education, Culture, Sports, Science and Technology (to M.Y.).

Appendix A. Supplementary data

Supplementary data associated with this article can be found, in the online version, at doi:10.1016/j.mrfmmm.2010.07.009.

References

[1] H. Weng, K. Morimoto, Differential responses to mutagens among human lymphocyte subpopulations, Mutat. Res. 672 (2009) 1–9.
[2] N. Holland, C. Bolognesi, M. Kirsch-Volders, S. Bonassi, E. Zeiger, S. Knasmueller, M. Fenech, The micronucleus assay in human buccal cells as a tool for biomonitoring DNA damage: the HUMN project perspective on current status and knowledge gaps, Mutat. Res. 659 (2008) 93–108.
[3] R. Mateuca, N. Lombaert, P.V. Aka, I. Decordier, M. Kirsch-Volders, Chromosomal changes: induction, detection methods and applicability in human biomonitoring, Biochimie 88 (2006) 1515–1531.
[4] M. Fenech, The in vitro micronucleus technique, Mutat. Res. 455 (2000) 81–95.
[5] R.A. El Zein, M.B. Schabath, C.J. Etzel, M.S. Lopez, J.D. Franklin, M.R. Spitz, Cytokinesis-blocked micronucleus assay as a novel biomarker for lung cancer risk, Cancer Res. 66 (2006) 6449–6456.
[6] S. Bonassi, A. Znaor, M. Ceppi, C. Lando, W.P. Chang, N. Holland, M. Kirsch-Volders, E. Zeiger, S. Ban, R. Barale, M.P. Bigatti, C. Bolognesi, A. Cebulska-Wasilewska, E. Fabianova, A. Fucic, L. Hagmar, G. Joksic, A. Martelli, L. Migliore, E. Mirkova, M.R. Scarfi, A. Zijno, H. Norppa, M. Fenech, An increased micronucleus frequency in peripheral blood lymphocytes predicts the risk of cancer in humans, Carcinogenesis 28 (2007) 625–631.
[7] A.K. Nersesyan, Possible role of the micronucleus assay in diagnostics and secondary prevention of cervix cancer: a minireview, Tsitol. Genet. 41 (2007) 64–66.
[8] D. Varga, W. Vogel, A. Bender, H. Surowy, C. Maier, R. Kreienberg, H. Deissler, G. Sauer, Increased radiosensitivity as an indicator of genes conferring breast cancer susceptibility, Strahlenther. Onkol. 183 (2007) 655–660.
[9] H.J. Evans, G.J. Neary, F.S. Williamson, The relative biological efficiency of single doses of fast neutrons and gamma-rays on Vicia faba roots and the effect of oxygen. Part II. Chromosone damage: the production of micronuclei, Int. J. Radiat. Biol. 1 (1959) 216–229.
[10] J.A. Heddle, A.V. Carrano, The DNA content of micronuclei induced in mouse bone marrow by gamma-irradiation: evidence that micronuclei arise from acentric chromosomal fragments, Mutat. Res. 44 (1977) 63–69.
[11] M. Hayashi, T. Sofuni, M. Ishidate Jr., Kinetics of micronucleus formation in relation to chromosomal aberrations in mouse bone marrow, Mutat. Res. 127 (1984) 129–137.
[12] H. Norppa, G.C. Falck, What do human micronuclei contain? Mutagenesis 18 (2003) 221–233.
[13] W.S. Saunders, M. Shuster, X. Huang, B. Gharaibeh, A.H. Enyenihi, I. Petersen, S.M. Gollin, Chromosomal instability and cytoskeletal defects in oral cancer cells, Proc. Natl. Acad. Sci. U.S.A. 97 (2000) 303–308.
[14] P. Thomas, K. Umegaki, M. Fenech, Nucleoplasmic bridges are a sensitive measure of chromosome rearrangement in the cytokinesis-block micronucleus assay, Mutagenesis 18 (2003) 187–194.
[15] X. Rao, Y. Zhang, Q. Yi, H. Hou, B. Xu, L. Chu, Y. Huang, W. Zhang, M. Fenech, Q. Shi, Multiple origins of spontaneously arising micronuclei in HeLa cells: direct evidence from long-term live cell imaging, Mutat. Res. 646 (2008) 41–49.
[16] D.R. Hoffelder, L. Luo, N.A. Burke, S.C. Watkins, S.M. Gollin, W.S. Saunders, Resolution of anaphase bridges in cancer cells, Chromosoma 112 (2004) 389–397.
[17] W. Rens, L. Torosantucci, F. Degrassi, M.A. Ferguson-Smith, Incomplete sister chromatid separation of long chromosome arms, Chromosoma 115 (2006) 481–490.
[18] K. Utani, J.K. Kawamoto, N. Shimizu, Micronuclei bearing acentric extrachromosomal chromatin are transcriptionally competent and may perturb the cancer cell phenotype, Mol. Cancer Res. 5 (2007) 695–704.
[19] B. Labidi, M. Gregoire, S. Frackowiak, D. Hernandez-Verdun, M. Bouteille, RNA polymerase activity in PtK1 micronuclei containing individual chromosomes. An in vitro and in situ study, Exp. Cell Res. 169 (1987) 233–244.
[20] H. Kato, A.A. Sandberg, Chromosome pulverization in human cells with micronuclei, J. Natl. Cancer Inst. 40 (1968) 165–179.
[21] M. Honma, M. Hayashi, T. Sofuni, Cytotoxic and mutagenic responses to X-rays and chemical mutagens in normal and p53-mutated human lymphoblastoid cells, Mutat. Res. 374 (1997) 89–98.
[22] M. Honma, M. Sakuraba, T. Koizumi, Y. Takashima, H. Sakamoto, M. Hayashi, Non-homologous end-joining for repairing I-SceI-induced DNA double strand breaks in human cells, DNA Repair (Amst) 6 (2007) 781–788.
[23] K. Sugimoto, T. Urano, H. Zushi, K. Inoue, H. Tasaka, M. Tachibana, M. Dotsu, Molecular dynamics of Aurora-A kinase in living mitotic cells simultaneously visualized with histone H3 and nuclear membrane protein importinalpha, Cell Struct. Funct. 27 (2002) 457–467.
[24] K. Sugimoto, K. Senda-Murata, S. Oka, Construction of three quadruple-fluorescent MDA435 cell lines that enable monitoring of the whole chromosome segregation process in the living state, Mutat. Res. 657 (2008) 56–62.
[25] B.A. Kruskal, C.H. Keith, F.R. Maxfield, Thyrotropin-releasing hormone-induced changes in intracellular [Ca2+] measured by microspectrofluorometry on individual quin2-loaded cells, J. Cell Biol. 99 (1984) 1167–1172.
[26] T. Matsushima, M. Hayashi, A. Matsuoka, M. Ishidate Jr., K.F. Miura, H. Shimizu, Y. Suzuki, K. Morimoto, H. Ogura, K. Mure, K. Koshi, T. Sofuni, Validation study of the in vitro micronucleus test in a Chinese hamster lung cell line (CHL/IU), Mutagenesis 14 (1999) 569–580.
[27] Y. Luan, T. Suzuki, R. Palanisamy, Y. Takashima, H. Sakamoto, M. Sakuraba, T. Koizumi, M. Saito, H. Matsufuji, K. Yamagata, T. Yamaguchi, M. Hayashi, M. Honma, Potassium bromate treatment predominantly causes large deletions, but not GC > TA transversion in human cells, Mutat. Res. 619 (2007) 113–123.
[28] N. Koyama, H. Sakamoto, M. Sakuraba, T. Koizumi, Y. Takashima, M. Hayashi, H. Matsufuji, K. Yamagata, S. Masuda, N. Kinae, M. Honma, Genotoxicity of acrylamide and glycidamide in human lymphoblastoid TK6 cells, Mutat. Res. 603 (2006) 151–158.
[29] N. Sato, K. Mizumoto, M. Nakamura, H. Ueno, Y.A. Minamishima, J.L. Farber, M. Tanaka, A possible role for centrosome overduplication in radiation-induced cell death, Oncogene 19 (2000) 5281–5290.
[30] K. Fukasawa, Centrosome amplification, chromosome instability and cancer development, Cancer Lett. 230 (2005) 6–19.
[31] Y Uetake, G. Sluder, Cell cycle progression after cleavage failure: mammalian somatic cells do not possess a "tetraploidy checkpoint", J. Cell Biol. 165 (2004) 609–615.
[32] M. Tomasz, Mitomycin C: small, fast and deadly (but very selective), Chem. Biol. 2 (1995) 575–579.
[33] J.H. Ford, C.J. Schultz, A.T. Correll, Chromosome elimination in micronuclei: a common cause of hypoploidy, Am. J. Hum. Genet. 43 (1988) 733–740.

Environmental and Molecular Mutagenesis 52:12–19 (2011)

Research Article

Genotoxicity of Acrylamide In Vitro: Acrylamide Is Not Metabolically Activated in Standard In Vitro Systems

Naoki Koyama,[1,2] Manabu Yasui,[1] Yoshimitsu Oda,[3] Satoshi Suzuki,[4] Tetsuo Satoh,[4] Takuya Suzuki,[5] Tomonari Matsuda,[5] Shuichi Masuda,[2] Naohide Kinae,[2] and Masamitsu Honma[1]*

[1]*Division of Genetics and Mutagenesis, National Institute of Health Sciences, 1-18-1 Kamiyoga, Setagaya-ku, Tokyo, Japan*
[2]*Laboratory of Food Hygiene, Graduate School of Food and Nutritional Sciences, University of Shizuoka, 52-1 Yada, Shizuaka-shi, Shizuoka, Japan*
[3]*Department of Applied Chemistry, Faculty of Science Engineering, Kinki University, 3-4-1, Kowakae, Higashiosaka-shi, Japan*
[4]*HAB Research Institute, Cornea Center Building, Ichikawa General Hospital, 5-11-13 Sugano, Ichikawa, Chiba, Japan*
[5]*Research Center for Environmental Quality Management, Kyoto University, 1-2 Yumihama, Otsu, Shiga, Japan*

The recent finding that acrylamide (AA), a genotoxic rodent carcinogen, is formed during the frying or baking of a variety of foods raises human health concerns. AA is known to be metabolized by cytochrome P450 2E1 (CYP2E1) to glycidamide (GA), which is responsible for AA's in vivo genotoxicity and probable carcinogenicity. In in-vitro mammalian cell tests, however, AA genotoxicity is not enhanced by rat liver S9 or a human liver microsomal fraction. In an attempt to demonstrate the in vitro expression of AA genotoxicity, we employed *Salmonella* strains and human cell lines that overexpress human CYP2E1. In the *umu* test, however, AA was not genotoxic in the CYP2E1-expressing *Salmonella* strain or its parental strain. Moreover, a transgenic human lymphoblastoid cell line overexpressing CYP2E1 (h2E1v2) and its parental cell line (AHH-1) both showed equally weak cytotoxic and genotoxic responses to high (>1 mM) AA concentrations. The DNA adduct N7-GA-Gua, which is detected in liver following AA treatment in vivo, was not substantially formed in the in vitro system. These results indicate that AA was not metabolically activated to GA in vitro. Thus, AA is not relevantly genotoxic in vitro, although its in vivo genotoxicity was clearly demonstrated. Environ. Mol. Mutagen. 52:12–19, 2011. © 2010 Wiley-Liss, Inc.

Key words: acrylamide; glycydamide; cytochrome P450 2E1 (CYP2E1), in vitro tests; *Salmonella*

INTRODUCTION

Recently, low levels of acrylamide (AA), a synthetic chemical widely used in industry, were detected in a variety of cooked foods [Tareke et al., 2000; Mottram et al., 2002]. It has been proposed that AA forms during frying and baking principally by the Maillard reaction between asparagine residues and glucose [Stadler et al., 2002; Tornqvist, 2005]. This finding raised concerns about a health risk for the general population [Tareke et al., 2002; Rice, 2005].

The International Agency for Research on Cancer classifies AA as 2A, a probable human carcinogen [IARC, 1994]. Because AA clearly induces gene mutations and micronuclei in mice, it could be a genotoxic carcinogen [Cao et al., 1993; Abramsson-Zetterberg, 2003; Manjanatha et al., 2005]. AA is metabolized by cytochrome P450 2E1 (CYP2E1) to glycidamide (GA), which can react with cellular DNA and protein [Sumner et al., 1999; Ghanayem et al., 2005a; Rice, 2005]. Two major

Grant sponsor: Health and Labor Sciences Research Grant, Japan; Grant Number: H21-food-general-012; Grant sponsor: Human Science Foundation, Japan; Grant Number: KHB1007.

*Correspondence to: Masamitsu Honma, Division of Genetics and Mutagenesis, National Institute of Health Sciences, 1-18-1 Kamiyoga, Setagaya-ku, Tokyo 158-8501, Japan. E-mail: honma@nihs.go.jp

Received 8 October 2009; provisionally accepted 5 January 2010; and in final form 19 January 2010

DOI 10.1002/em.20560

Published online 7 March 2010 in Wiley Online Library (wileyonlinelibrary.com).

© 2010 Wiley-Liss, Inc.

GA-DNA adducts, N7-(2-carbamoyl-2-hydroxyethyl)-guanine (N7-GA-Gua) and N3-(2-carbamoyl-2-hydroxyethyl)-adenine (N3-GA-Ade), have been identified in mice and rats treated with AA or GA [Segerback et al., 1995; Gamboa da Costa et al., 2003; Doerge et al., 2005], with the level of N7-GA-Gua being 100 times as high as the level of N3-GA-Ade in the test organ [Gamboa da Costa et al., 2003]. It is likely that these DNA adducts are responsible for AA's in vivo genotoxicity [Carere, 2006; Ghanayem and Hoffler, 2007]. In our previous study, however, AA did not induce micronuclei in human lymphoblastoid TK6 cells in the presence of rat liver S9, although the genotoxicity of *N*-di-*N*-butylnitrosamine (DBN), which is also metabolized by CYP2E1, was enhanced under the same conditions [Koyama et al., 2006]. Other in vitro genotoxicity studies have also failed to demonstrate the metabolic activation of AA in the presence of S9 [Knaap et al., 1988; Tsuda et al., 1993; Dearfield et al., 1995; Friedman, 2003]. It may be because most S9 preparations have low CYP2E1 activity [Calleman et al., 1990; Hargreaves et al., 1994].

In an attempt to demonstrate the genotoxicity of AA in vitro, we tested the compound using bacteria and mammalian cell lines that express CYP2E1. *S. typhimurium* OY1002/2E1 strain expresses respective human CYP2E1 enzyme and NADPH-cytochrome P450 reductase (reductase), and bacterial *O*-acetyltransferase [Oda et al., 2001]. Using the strain, as well as its parental strain not expressing these enzymes, we conducted an *umu* assay to evaluate induction of cytotoxicity and DNA damage by AA relative to that induced by its metabolite GA. The principle of the *umu* assay is based on the ability of the DNA-damaging agents inducing the *umu* operon. Monitoring the levels of *umu* operon expression enables us to quantitatively detect environmental mutagens [Oda et al., 1985]. In addition, we evaluated the relative mutagenicity of AA vs. GA in assays using transgenic human lymphoblastoid cell lines. Induction of gene mutation at the *TK* locus and of chromosome damage leading to micronucleus (MN) formation were assessed in the h2E1v2 which overexpress human CYP2E1 [Crespi et al., 1993a], vs. its parental cell line, AHH-1. We also investigated the relationship between AA genotoxicity and the formation N7-GA-Gua (derived from GA) in the in vitro mammalian cell system.

MATERIALS AND METHODS

Bacterial Strains, Cell Lines, Chemicals, and Human Liver Microsomal Fraction

For the bacterial tests, we used *umu* strain *S. typhimurium* OY1002/2E1, which expresses human CYP2E1, reductase, and bacterial *O*-acetyltransferase, and its parental strain, *S. typhimurium* TA1535/pSK1002 that does not express these enzymes [Oda et al., 2001].

For the mammalian cell tests, we used human lymphoblastoid cell lines, TK6, AHH-1, and h2E1v2. The TK6 cell line has been described previously [Honma et al., 1997]. The AHH-1 and h2E1v2 cell lines were kindly gifted from Dr. Charles Crespi (BD Bio Sciences, Bedford, MA). AHH-1 is a clonal isolate, derived from RPMI 1788 cells, which was selected for sensitivity to benzo[*a*]pyrene [Crespi and Thilly, 1984]. AHH-1 shows high activity of endogenous CYP1A1. Heterozygosity of AHH-1 cells at thymidine kinase (TK) locus was derived in a two-step selection process utilizing the frameshift mutagen, ICR-191. The AHH-1 cell line was then transfected with plasmids encoding human CYP2E1 enzymes, generating h2E1v2 cell line. AHH-1 expresses CYP1A1 and h2E1v2 expresses both CYP1A1 and CYP2E1 [Crespi et al., 1993a,b].

We purchased AA (CAS No. 79-06-1) and GA (CAS No. 5694-00-8) from Wako Pure Chemical (Tokyo) and dissolved them in phosphate-buffered saline just before use. We purchased *N*-di-*N*-methylnitorosamine (DMN) (CAS No. 62-75-9) from Sigma Aldrich Japan (Tokyo) and dissolved it in DMSO as a positive control for use. We purchased liver S9 prepared from SD rats treated with phenobarbital and 5,6-benzoflavone from the Oriental Yeast (Tokyo). The human liver S9 (HLS-104) was prepared from a human liver sample, which was legally procured from the NDRI (National Disease Research Interchange) in Philadelphia, USA, with permission to use for research purpose only. HLS-104 showed high activity of CYP2E1 [Hakura et al., 2005]. We prepared microsomal fraction from the S9 according to an established procedure [Suzuki et al., 2000]. We prepared the S9- or microsome-mix by mixing 4 ml S9 or microsomal fraction with 2 ml each of 180 mg/ml glucose-6-phosphate, 25 mg/ml NADP, and 150 mM KCl. CYP2E1 activity of the S9 and microsomal fractions were determined as the activity of chlorzaxazone 6-hydroxylation according to the method of Ikeda et al. [2001].

We grew the cell lines in RPMI1640 medium (Gibco-BRL, Life Technology, Grand Island, NY) supplemented with 10% heat-inactivated horse serum (JRH Biosciences, Lenexa, KS), 200 μg/ml sodium pyruvate, 100 U/ml penicillin, and 100 μg/ml streptomycin, and we maintained the cultures at 10^5-10^6 cells/ml at 37°C in a 5% CO_2 atmosphere with 100% humidity.

umu Assay

The *umu* assay was carried out by the method of Aryal et al. [1999, 2000] with slight modification. Overnight cultures of tester strains were diluted 100-fold with TGlyT medium (1% Bactotryptone, 0.5% NaCl (w/v), 0.2% glycerol (v/v), and 1 μg of tetracycline/ml, 1.0 mM IPTG, 0.5 mMδ-ALA, and 250 ml of trace element mixture/l) [Sandhu et al., 1994]. The culture was incubated for 1 hr at 37°C and then 0.75 ml aliquots of TGA culture (OD_{600}: 0.25–0.3) and human. Induction of the *umu*C gene by HCAs in different strains was determined by measuring cellular β-galactosidase activity, as described by Oda et al. [1985]. Cell toxicity was determined in reaction mixture by measuring the optical density change at 600 nm.

Mammalian Cell Assays Measuring Gene Mutation and Chromosome Damage

We incubated 20-ml aliquots of TK6, AHH-1, or h2E1v2 cell suspensions (5.0×10^5 cells/ml) treated with serially diluted AA, GA, or DMN in the presence or absence of S9 or micorosomes at 37°C for 4 hr, washed them once, resuspended them in fresh medium, and cultured them in new flasks for the MN and TK assays. For TK6 cells, we also seeded cells into the 96-well plates (1.6 cells/well) to determine plating efficiency (PE0).

Forty-eight hours after treating the cells, we prepared the MN test samples as previously reported [Koyama et al., 2006]. At least, 1,000 intact interphase cells for each treatment were examined, and the cells containing MN were scored. The MN frequencies between nontreated and treated cells were statistically analyzed by Fisher's exact test. The concentration–response relationship was evaluated by the Cochran-Armitage trend test [Matsushima et al., 1999].

We maintained the cultures another 24 hr to allow phenotypic expression prior to plating for determination of the mutant fractions. After the expression time, to isolate the TK deficient mutants, we seeded the cells into 96-well plates in the presence of 3.0 μg/ml trifluorothymidine (TFT).

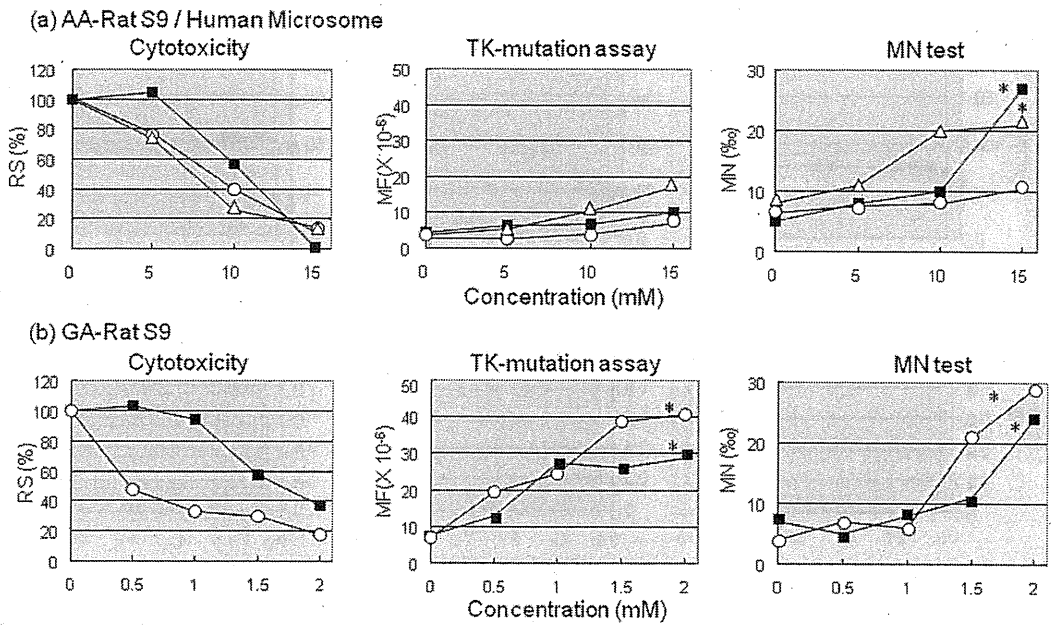

Fig. 1. Cytotoxic (relative survival, RS) and genotoxic (TK and MN assays) responses of TK6 cells treated with AA or GA for 4 hr with or without metabolic activation. (a) TK6 cells were treated with AA without (■) or with (○) rat liver S9 or human microsomes (△). (b) TK6 cells were treated with GA without (■) or with (○) rat liver S9. *$P < 0.05$ (Omori method for TK-mutation assay, trend test for MN assay).

We also seeded cells into the 96-well plates in the absence of TFT to determine plating efficiency (PE3). TK6 cells were seeded at 40,000 cells/well and 1.6 cell/well for TFT and PE plates, respectively. AHH-1 and h2E1v2 cells were seeded at 5,000 cells/well and 3.2 cells/well for TFT and PE plates, respectively. All plates were incubated at 37°C in 5% CO_2 in a humidified incubator. We scored for the colonies in the PE plates at 14th day after plating, and scored for the colonies in the TFT plate on the 28th day after plating. Mutation frequencies were calculated according to the Poisson distribution [Furth et al., 1981]. The data were statistically analyzed by Omori's method, which consists of a modified Dunnett's procedure for identifying clear negative, a Simpson-Margolin procedure for detecting downturn data, and a trend test to evaluate the dose-dependency [Omori et al., 2002]. We evaluated cytotoxicity for TK6 by relative survival (RS), which is calculated from plating efficiency (PE0), and for AHH-1 and h2E1v2 by relative suspension growth (RSG), which is calculated from cell growth rate during 3 days expression period.

Western Blot Analysis

A goat polyclonal anti-rat CYP2E1 antibody (Daiichi Pure Chemical, Tokyo) and rabbit anti-rat actin (Sigma, St. Louis, MO) were used as primary antibodies. AP-conjugated secondary antibody (Cappel, Organon Technika Corp., West Chester, PA) was used to detect primary antibody signals.

DNA Adduct Assay

As a standard for LC/MS/MS analysis, N7-GA-Gua and [$^{15}N_5$]-labeled N7-GA-Gua were synthesized as described previously [Gamboa da Costa et al., 2003]. DNA was extracted from the cells by using DNeasy 96 Blood &Tissue Kit (QIAGEN, Düsseldorf) and incubated at 37°C for 48 hr for deprination. An aliquot of the [$^{15}N_5$]-labeled N7-GA-Gua standard was added to each sample and filtered through an ultrafiltration membrane to remove DNA. The eluted-solution was evaporated thoroughly and dissolved in water, and then the solutions were subsequently quantified by LC/MS/MS.

RESULTS

Cytotoxicity and Genotoxicity of AA and GA Under Metabolic Activation

We used human microsomal preparation and phenobarbital- and 5,6-benzoflavone-treated rat liver S9 for metabolic activation. CYP2E1 activity of the human microsomal preparation was more than twice that of the rat liver S9 preparations (2,917 vs. 1,295 pmol/mg/min).

Figure 1 shows the cytotoxicity (RS; relative survival), MN, and *TK*-mutations induced by AA (a) and GA (b) with and without rat liver S9 or human microsomes. Rat liver S9 or human microsomes enhanced cytotoxicity (RS) of AA and GA. On the other hand, AA showed weak genotoxicity only at relatively high concentrations (>10 mM) without S9, but neither activating system enhanced the weak genotoxicty. GA induced TK-mutations dose-dependently from the low concentration (0.5 mM) and induced MN from 1.5 mM both with and without S9. Thus, neither the rat nor human metabolizing system activated AA or inhibited the expression of GA genotoxicity.

umu Assay Using Strains Expressing Human CYP2E1

We used *S. typhimurium* OY1002/2E1 strain to assess the cell toxicity and genotoxicity of AA at exposures up to 10mM (Fig. 2c). We also examined AA and GA with

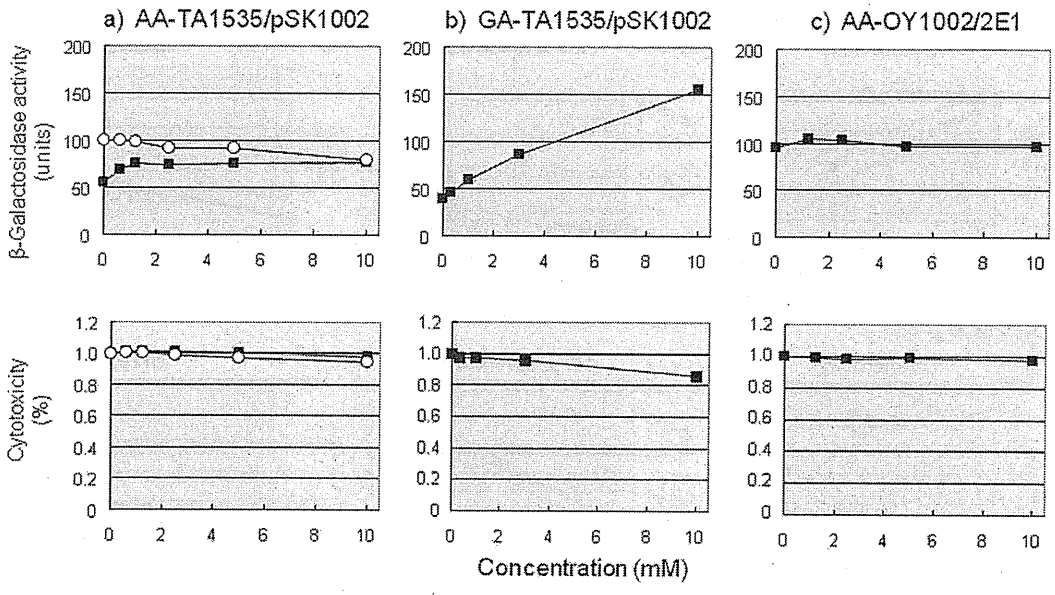

Fig. 2. Induction of *umuC* gene expression and cytotoxic response by AA (**a**, **c**) or GA (**b**) in *S. typhimurium* tester strains TA1535/pSK1002 (a, b) and OY1002/2E1 (c). The *umu* tests were conducted without (■) or with rat S9 (○). β-Galactosidase activity (units) was determined as described in Materials and Methods. Cytotoxic activities are expressed as % optical density change at 600 nm.

or without rat S9 using TA1535/pSK1002 strain. Although GA clearly produced a dose-related increase in response to DNA damage (Fig. 2b), AA elicited no genotoxic or cell toxic response with and without S9 (Fig. 2a). Thus, we could not demonstrate any in vitro genotoxicity of AA in the bacterial system.

Cytotoxic and Genotoxic Responses to AA in Transgenic Cell Lines

Western blot analysis revealed that h2E1v2 accumulated more CYP2E1 than either of its parental cell lines (Fig. 3). Both the h2E1v2 and AHH-1 cells exhibited weak responses (TK-gene mutations and MN) to AA at ≤3 mM with little difference in cytotoxicity (RSG, relative suspension growth) (Fig. 4a). h2E1v2 differed from AHH-1, however, in that it showed clear genotoxic and cytotoxic responses (RSG) to DMN, which is a representative substrate for CYP2E1 (Fig. 4b). Thus, the h2E1v2 cell line had CYP2E1 activity but did not activate AA.

DNA Adduct Formation by AA and GA in the Cell Lines

AA induced trace amounts of N7-GA-Gua adduct in TK6 cells (with and without S9) (Fig. 5a) and in AHH-1 and h2E1v2 cells (Fig. 5b). GA, on the other hand, induced a substantial number of N7-GA-Gua adducts in TK6 cells (Fig. 5c). These results suggest that the expression of genotoxicity may be dependent on N7-GA-Gua adduct formation, and the in vitro metabolic activation system did not metabolize AA into GA.

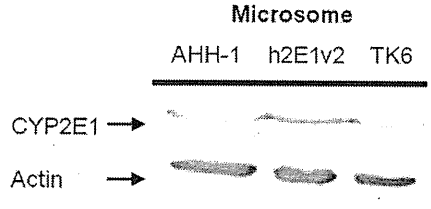

Fig. 3. Western blot analysis of CYP2E1 in AHH-1, h2E1v2, and TK6 cells. Equal amount of materials were loaded for each sample. CYP2E1 protein was stained with the anti-CYP2E1 antibody. Actin was used as a loading control.

DISCUSSION

A large number of studies about the in vitro genotoxicity of AA have been reported [Dearfield et al., 1995; Besaratinia and Pfeifer, 2005]. AA was negative in Ames assay in both the presence and absence of S9 [Zeiger et al., 1987; Knaap et al., 1988; Tsuda et al., 1993]. In mammalian cell assays, cytogenetic tests such as chromosome aberration test and sister chromatid exchange tests were positive [Sofuni et al., 1985; Tsuda et al., 1993]. AA also induced *Tk* mutation in the MLA but did not induce *Hprt* mutation in V79 cells [Moore et al., 1987;

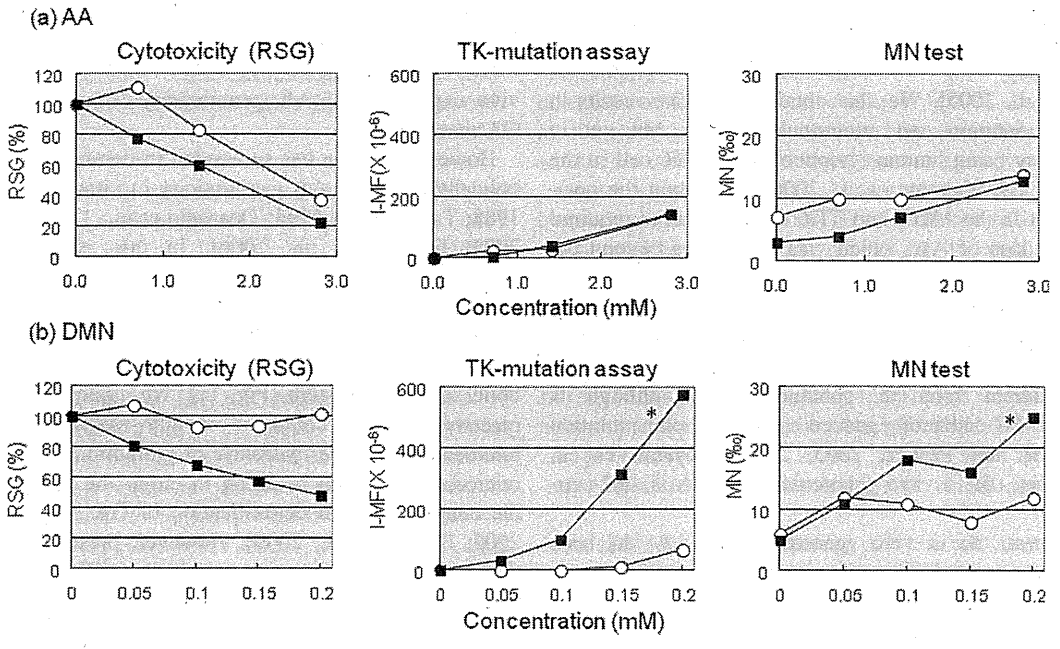

Fig. 4. Cytotoxic (relative suspension growth, RSG) and genotoxic (TK assay and MN test) responses of AHH-1 (○) or h2E1v2 (■) cells treated with AA or DMN for 4 hr. I-MF means induced mutation fraction, in which back ground mutation frequency is subtracted. *$P < 0.05$ (Omori method for TK-mutation assay, trend test for MN assay).

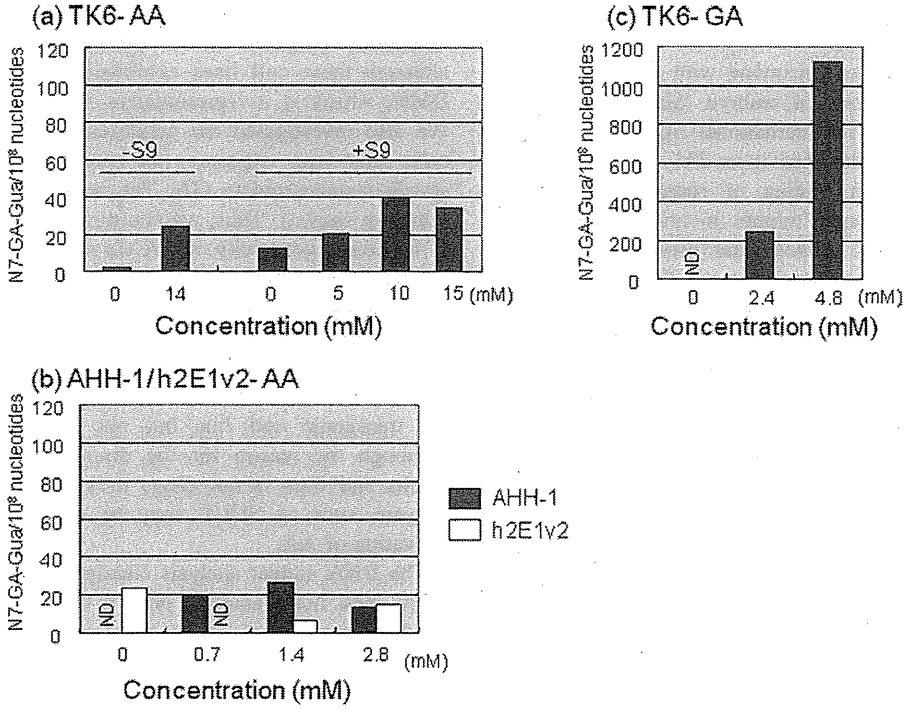

Fig. 5. Levels of N7-GA-Gua adduct in TK6 (**a**, **c**), AHH-1 (**b**), or h2E1v2 (b) cells treated with AA (a, b) or GA (c) for 4 hr at different concentrations. Data are expressed as the number of adducts in 10^8 nucleotides.

Knaap et al., 1988; Tsuda et al., 1993; Baum et al., 2005; Mei et al., 2008], and produced negative results in the Comet assay with V79 cells and human lymphocytes [Baum et al., 2005]. We also obtained positive results in *TK* gene mutation and micronuclei assays, but not in Comet assay using human lymphoblastoid TK6 cell in the absence of S9 [Koyama et al., 2006]. To obtain the positive results in the MLA and TK6 cells, however required very high dose of AA, which was sometimes beyond the top dose of the OECD testing guideline (>10 mM) [Koyama et al., 2006; Mei et al., 2008]. The spectrum of AA-induced *TK* mutations in TK6 and *cII* mutations in Big Blue® mouse embryonic fibroblasts were not significantly different from the spontaneous one, although its metabolite GA distinctly induced a specific point mutation [Besaratinia and Pfeifer, 2003, 2004; Koyama et al., 2006]. Thus, the in vitro genotoxicity of AA is still controversial.

In contrast, the in vivo genotoxicity of AA has been clearly demonstrated by various rodent genotoxicity tests including micronuclei tests in peripheral blood [Cao et al., 1993; Abramsson-Zetterberg, 2003; Manjanatha et al., 2005], transgenic gene mutation in liver [Manjanatha et al., 2005], and Comet assay in various organs [Ghanayem et al., 2005b]. AA has also proven to be genotoxic to germ cells [Dearfield et al., 1995]. AA induced micronuclei in mice spermatids, and heritable chromosome translocations and specific locus mutations in postomeiotic sperm and spermatogonia [Lahdetie et al., 1994; Xiao and Tates, 1994]. AA also elevated the frequency of dominant lethal mutations probably accompanying with chromosome aberrations leading to death of embryo [Shelby et al., 1987; Adler et al., 1994]. The International Agency for Research on Cancer (IARC) classified it as 2A, a probable human carcinogen based on finding of rodent carcinogenicity [IARC, 1994]. AA caused tumors in various organs including mammary gland, peritesticular mesothelium, thyroid, and central nervous system [Carere, 2006], although the AA-inducing genotoxicity in these organs have not been demonstrated.

AA is metabolized either via direct glutathione conjugation followed by excretion of mercapturic acid or via oxidative pathways catalyzed by CYP2E1 to yield GA [Calleman et al., 1990; Wu et al., 1993; Sumner et al., 1999]. GA reacts quickly with DNA, mainly forming N7-GA-Gua adduct. Genotoxicity of GA has been demonstrated in vitro and in vivo. In contrast to AA, GA is positive in most genotoxicity tests [Hashimoto and Tanii, 1985; Dearfield et al., 1995; Besaratinia and Pfeifer, 2004; Baum et al., 2005; Koyama et al., 2006]. Manjanatha et al. [2005] demonstrated in transgenic Big Blue® mice that both AA and GA induces endogenous *Hprt* and transgenic *cII* mutation at same level, and also produced similar mutational spectra. The predominant type of mutations observed in these two systems was G:C to T:A transversion, which is presumably derived from N7-GA-Gua [Besaratinia and Pfeifer, 2005]. The in vivo results with transgenic Big Blue® mice indicate that in vivo expression of AA genotoxicity is mediated via its GA metabolite.

However, no one has succeeded in demonstrating metabolically activated AA genotoxicity in vitro [Knaap et al., 1988; Tsuda et al., 1993; Dearfield et al., 1995; Friedman, 2003; Emmert et al., 2006]. In this study, we used induced rat liver S9 and human microsomal fraction for the metabolic activation. Although they have high CYP2E1 activity, the AA-inducing genotoxicity was never influenced by the presence of the exogenous metabolic activation system (Fig. 1a). We assumed that GA, a reactive epoxide, could be rapidly inactivated through microsomal epoxide hydrolase or glutathione in any S9 or microsomal fraction resulting in either the metabolism or the conjugation and detoxification of GA [Sumner et al., 2003; Decker et al., 2009]. However, presence of rat S9 did not prevent GA from inducing *TK*-mutation and micronuclei.

The *umu* assay could not detect the genotoxicity of AA even by the strain (Fig. 2). Emmert et al. [2006] also failed to demonstrate the mutagenicity of AA in the Ames test using the metabolically competent *S. typhimurium strain* YG7108pinERb_5 that expresses CYP2E1. In mammalian cell system, such as the human lymphoblastoid cell line, h2E1v2 overexpressing human CYP2E1 did not show different response in *TK*-gene mutation and MN induction compared to its parental cell line, AHH-1, although these cell lines exhibited distinct difference to DMN, which is a representative substrate for CYP2E1. We also investigated the genotoxicity of AA in h2E1v2 cells after long exposure (24 hr), because AA may be slowly metabolized to GA. The result was also negative (data not shown). Thus, we could not obtain any evidence of in vitro genotoxicity of AA *via* metabolic activation.

Glatt et al. [2005] developed a Chinese hamster V79-derived cell line that stably expresses human CYP2E1 and sulphotransferase (SULT), and applied it to investigate sister chromatid exchanges (SCE) induced by some chemicals. They demonstrated that AA induced SCE in the transgenic cell line but not in the parental line. Although the reason for the discrepancy between their results and ours is not clear, it is possible that another enzyme, such as SULT, may be involved in metabolic activation of AA.

The DNA adduct analysis clearly revealed that h2E1v2 cells does not generate N7-GA-Gua adduct in vitro. Because exposure of human cells to GA results in significant accumulation of N7-GA-Gua adduct, but DNA adduct analysis following exposure of h2E1v2 with AA does not generate N7-GA-Gua adduct in vitro, lead one a conclusion that the presence of CYP2E1 alone is not enough to metabolize AA to GA in mammalian cells. The

DNA adduct analysis also strongly supports a hypothesis that GA contribute to its genotoxicity by forming N7-GA-Gua adduct. Interestingly, very small amount of N7-GA-Gua adduct was generated in TK6 cells in a dose-dependent manner regardless of the presence of S9 (Fig. 5a). TK6 cells themselves may have an enzymatic activity to metabolize AA to GA, although its activity must be extremely low. Ghanayem et al. [2005b] showed that AA was not mutagenic or genotoxic in CYP2E1-null mice. Intraperitoneal injection of AA (25, 50 mg/kg) by once daily for 5 days induced micronuclei in erythrocyte and DNA damage assessed by Comet assay in leukocyte and liver cells of wild-type, but not in the CYP2E1-null mice. The plasma concentration of AA in the CYP2E1-null mice was 115-times higher than in the wild-type mice, while the GA concentration in the CYP2E1-null mice was negligible compared to that in the wild-type mice [Ghanayem et al., 2000]. Ghanayem et al. [2005c] also demonstrated that AA produces dominant lethal in mice that express CYP2E1, but not in mice that do not express CYP2E1, indicating that induction of germ cell mutations by AA in mice in vivo is also dependent upon CYP2E1 metabolism. These results clearly suggest that CYP2E1 is the principal enzyme responsible for the metabolism of AA to GA in vivo.

In conclusion, AA could not be metabolized to GA by in vitro metabolic activation system commonly used in genotoxicity tests. In vivo, on the other hand, GA is apparently responsible for AA-inducing genotoxicity. Although AA may exhibit genotoxicity in in vitro mammalian cells at high concentrations, its positive response is not relevant for its major genotoxicity. AA could be classified into in vivo specific genotoxic chemical.

ACKNOWLEDGMENT

We thank Dr. Crespi (BD Bio Sciences) for kindly providing the AHH-1 and h2E1v2 cell lines.

REFERENCES

Abramsson-Zetterberg L. 2003. The dose-response relationship at very low doses of acrylamide is linear in the flow cytometer-based mouse micronucleus assay. Mutat Res 535:215–222.

Adler ID, Reitmeir P, Schmoller R, Schriever-Schwemmer G. 1994. Dose response for heritable translocations induced by acrylamide in spermatids of mice. Mutat Res 309:285–291.

Aryal P, Yoshikawa K, Terashita T, Guengerich FP, Shimada T, Oda Y. 1999. Development of a new genotoxicity test system with *Salmonella typhimurium* OY1001/1A2 expressing human CYP1A2 and NADPH-P450 reductase. Mutat Res 442:113–120.

Aryal P, Terashita T, Guengerich FP, Shimada T, Oda Y. 2000. Use of genetically engineered *Salmonella typhimurium* OY1002/1A2 strain coexpressing human cytochrome P450 1A2 and NADPH-cytochrome P450 reductase and bacterial *O*-acetyltransferase in SOS/umu assay. Environ Mol Mutagen 36:121–126.

Baum M, Fauth E, Fritzen S, Herrmann A, Mertes P, Merz K, Rudolphi M, Zankl H, Eisenbrand G. 2005. Acrylamide and glycidamide: Genotoxic effects in V79-cells and human blood. Mutat Res 580:61–69.

Besaratinia A, Pfeifer GP. 2003. Weak yet distinct mutagenicity of acrylamide in mammalian cells. J Natl Cancer Inst 95:889–896.

Besaratinia A, Pfeifer GP. 2004. Genotoxicity of acrylamide and glycidamide. J Natl Cancer Inst 96:1023–1029.

Besaratinia A, Pfeifer GP. 2005. DNA adduction and mutagenic properties of acrylamide. Mutat Res 580:31–40.

Calleman CJ, Bergmark E, Costa LG. 1990. Acrylamide is metabolized to glycidamide in the rat: Evidence from hemoglobin adduct formation. Chem Res Toxicol 3:406–412.

Cao J, Beisker W, Nusse M, Adler ID. 1993. Flow cytometric detection of micronuclei induced by chemicals in poly- and normochromatic erythrocytes of mouse peripheral blood. Mutagen 8:533–541.

Carere A. 2006. Genotoxicity and carcinogenicity of acrylamide: A critical review. Ann Ist Super Sanita 42:144–155.

Crespi CL, Thilly WG. 1984. Assay for gene mutation in a human lymphoblast line, AHH-1, competent for xenobiotic metabolism. Mutat Res 128:221–230.

Crespi CL, Langenbach R, Penman BW. 1993a. Human cell lines, derived from AHH-1 TK+/- human lymphoblasts, genetically engineered for expression of cytochromes P450. Toxicology 82:89–104.

Crespi CL, Penman BW, Gonzalez FJ, Gelboin HV, Galvin M, Langenbach R. 1993b. Genetic toxicology using human cell lines expressing human P-450. Biochem Soc Trans 21:1023–1028.

Dearfield KL, Douglas GR, Ehling UH, Moore MM, Sega GA, Brusick DJ. 1995. Acrylamide: A review of its genotoxicity and an assessment of heritable genetic risk. Mutat Res 330:71–99.

Decker M, Arand M, Cronin A. 2009. Mammalian epoxide hydrolases in xenobiotic metabolism and signalling. Arch Toxicol 83:297–318.

Doerge DR, da Costa GG, McDaniel LP, Churchwell MI, Twaddle NC, Beland FA. 2005. DNA adducts derived from administration of acrylamide and glycidamide to mice and rats. Mutat Res 580:131–141.

Emmert B, Bunger J, Keuch K, Muller M, Emmert S, Hallier E, Westphal GA. 2006. Mutagenicity of cytochrome P450 2E1 substrates in the Ames test with the metabolic competent *S. typhimurium* strain YG7108pin3ERb5. Toxicology 228:66–76.

Friedman M. 2003. Chemistry, biochemistry, and safety of acrylamide. A review. J Agric Food Chem 51:4504–4526.

Furth EE, Thilly WG, Penman BW, Liber HL, Rand WM. 1981. Quantitative assay for mutation in diploid human lymphoblasts using microtiter plates. Anal Biochem 110:1–8.

Gamboa da Costa G, Churchwell MI, Hamilton LP, Von Tungeln LS, Beland FA, Marques MM, Doerge DR. 2003. DNA adduct formation from acrylamide via conversion to glycidamide in adult and neonatal mice. Chem Res Toxicol 16:1328–1337.

Ghanayem BI, Hoffler U. 2007. Investigation of xenobiotics metabolism, genotoxicity, and carcinogenicity using Cyp2e1(-/-) mice. Curr Drug Metab 8:728–749.

Ghanayem BI, Wang H, Sumner S. 2000. Using cytochrome P-450 gene knock-out mice to study chemical metabolism, toxicity, and carcinogenicity. Toxicol Pathol 28:839–850.

Ghanayem BI, McDaniel LP, Churchwell MI, Twaddle NC, Snyder R, Fennell TR, Doerge DR. 2005a. Role of CYP2E1 in the epoxidation of acrylamide to glycidamide and formation of DNA, hemoglobin adducts. Toxicol Sci 88:311–318.

Ghanayem BI, Witt KL, Kissling GE, Tice RR, Recio L. 2005b. Absence of acrylamide-induced genotoxicity in CYP2E1-null mice: Evidence consistent with a glycidamide-mediated effect. Mutat Res 578:284–297.

Ghanayem BI, Witt KL, El-Hadri L, Hoffler U, Kissling GE, Shelby MD, Bishop JB. 2005c. Comparison of germ cell mutagenicity in male CYP2E1-null and wild-type micetreated with acrylamide: Evidence supporting a glycidamide-mediated effect. Biol Reprod 72:157–163.

Glatt H, Schneider H, Liu Y. 2005. V79-hCYP2E1-hSULT1A1, a cell line for the sensitive detection of genotoxic effects induced by carbohydrate pyrolysis products and other food-borne chemicals. Mutat Res 580:41–52.

Hakura A, Shimada H, Nakajima M, Sui H, Kitamoto S, Suzuki S, Satoh T. 2005. Salmonella/human S9 mutagenicity test: A collaborative study with 58 compounds. Mutagen 20:217–228.

Hargreaves MB, Jones BC, Smith DA, Gescher A. 1994. Inhibition of *p*-nitrophenol hydroxylase in rat liver microsomes by small aromatic and heterocyclic molecules. Drug Metab Dispos 22: 806–810.

Hashimoto K, Tanii H. 1985. Mutagenicity of acrylamide and its analogues in *Salmonella typhimurium*. Mutat Res 158:129–133.

Honma M, Hayashi M, Sofuni T. 1997. Cytotoxic and mutagenic responses to X-rays and chemical mutagens in normal and p53-mutated human lymphoblastoid cells. Mutat Res 374:89–98.

IARC. Acrylamide. In:IARC Monographs on the Evaluation of Carcinogen Risk to Human: Some Industrial Chemicals, Vol. 60. Lyon: International Agency for Research on Cancer. Lyon. 1994. pp 389–433.

Ikeda T, Nishimura K, Taniguchi T. 2001. In vitro evaliation of drug interaction caused by enzyme inhibition-HAB protocol. Xenobiol Metabol Dispos 16:115–126.

Knaap AG, Kramers PG, Voogd CE, Bergkamp WG, Groot MG, Langebroek PG, Mout HC, van der Stel JJ, Verharen HW. 1988. Mutagenic activity of acrylamide in eukaryotic systems but not in bacteria. Mutagen 3:263–268.

Koyama N, Sakamoto H, Sakuraba M, Koizumi T, Takashima Y, Hayashi M, Matsufuji H, Yamagata K, Masuda S, Kinae N, Honma M. 2006. Genotoxicity of acrylamide and glycidamide in human lymphoblastoid TK6 cells. Mutat Res 603:151–158.

Lahdetie J, Suutari A, Sjoblom T. 1994. The spermatid micronucleus test with the dissection technique detects the germ cell mutagenicity of acrylamide in rat meiotic cells. Mutat Res 309:255–262.

Manjanatha MG, Aidoo A, Shelton SD, Bishop ME, MacDaniel LP, Doerge DR. 2005. Evaluation of mutagenicity in Big Blue (BB) mice administred acrylamide (AA) and glycidamide (GA) in drinking water for 4 weeks. Environ Mol Mutagen 44:214.

Matsushima T, Hayashi M, Matsuoka A, Ishidate M Jr, Miura KF, Shimizu H, Suzuki Y, Morimoto K, Ogura H, Mure K, Koshi K, Sofuni T. 1999. Validation study of the in vitro micronucleus test in a Chinese hamster lung cell line (CHL/IU). Mutagen 14:569–580.

Mei N, Hu J, Churchwell MI, Guo L, Moore MM, Doerge DR, Chen T. 2008. Genotoxic effects of acrylamide and glycidamide in mouse lymphoma cells. Food Chem. Toxicol 46:628–636.

Moore MM, Amtower A, Doerr C, Brock KH, Dearfield KL. 1987. Mutagenicity and clastogenicity of acrylamide in L5178Y mouse lymphoma cells. Environ Mutagen 9:261–267.

Mottram DS, Wedzicha BL, Dodson AT. 2002. Acrylamide is formed in the Maillard reaction. Nature 419:448–449.

Oda Y, Nakamura S, Oki I, Kato T, Shinagawa H. 1985. Evaluation of the new system (umu-test) for the detection of environmental mutagens and carcinogens. Mutat Res 147:219–229.

Oda Y, Aryal P, Terashita T, Gillam EM, Guengerich FP, Shimada T. 2001. Metabolic activation of heterocyclic amines and other procarcinogens in *Salmonella typhimurium* umu tester strains expressing human cytochrome P4501A1, 1A2, 1B1, 2C9, 2D6, 2E1, and 3A4 and human NADPH-P450 reductase and bacterial *O*-acetyltransferase. Mutat Res 492:81–90.

Omori T, Honma M, Hayashi M, Honda Y, Yoshimura I. 2002. A new statistical method for evaluation of L5178Ytk(+/−) mammalian cell mutation data using microwell method. Mutat Res 517:199–208.

Rice JM. 2005. The carcinogenicity of acrylamide. Mutat Res 580:3–20.

Sandhu P, Guo Z, Baba T, Martin MV, Tukey RH, Guengerich FP. 1994. Expression of modified human cytochrome P450 1A2 in *Escherichia coli*: Stabilization, purification, spectral characterization, and catalytic activities of the enzyme. Arch Biochem Biophys 309:168–177.

Segerback D, Calleman CJ, Schroeder JL, Costa LG, Faustman EM. 1995. Formation of *N*-7-(2-carbamoyl-2-hydroxyethyl)guanine in DNA of the mouse and the rat following intraperitoneal administration of [14C]acrylamide. Carcinogenesis 16:1161–1165.

Shelby MD, Cain KT, Cornett CV, Generoso WM. 1987. Acrylamide: Induction of heritable translocation in male mice. Environ Mutagen 9:363–368.

Sofuni T, Hayashi M, Matsuoka A, Sawada M. 1985. Mutagenicity tests on organic chemical concominants in city water and related compounds. II. Chromosome aberration tests in cultured mammalian cells. Eisei Shiken Hok 103:64–75.

Stadler RH, Blank I, Varga N, Robert F, Hau J, Guy PA, Robert MC, Riediker S. 2002. Acrylamide from Maillard reaction products. Nature 419:449–450.

Sumner SC, Fennell TR, Moore TA, Chanas B, Gonzalez F, Ghanayem BI. 1999. Role of cytochrome P450 2E1 in the metabolism of acrylamide and acrylonitrile in mice. Chem Res Toxicol 12:1110–1116.

Sumner SC, Williams CC, Snyder RW, Krol WL, Asgharian B, Fennell TR. 2003. Acrylamide: A comparison of metabolism and hemoglobin adducts in rodents following dermal, intraperitoneal, oral, or inhalation exposure. Toxicol Sci 75:260–270.

Suzuki S, Kurata N, Nishimura Y, Yasuhara H, Satoh T. 2000. Effects of imidazole antimycotics on the liver microsomal cytochrome P450 isoforms in rats: Comparison of in vitro and ex vivo studies. Eur J Drug Metab Pharmacokinet 25:121–126.

Tareke E, Rydberg P, Karlsson P, Eriksson S, Tornqvist M. 2000. Acrylamide: A cooking carcinogen? Chem Res Toxicol 13:517–522.

Tareke E, Rydberg P, Karlsson P, Eriksson S, Tornqvist M. 2002. Analysis of acrylamide, a carcinogen formed in heated foodstuffs. J Agric Food Chem 50:4998–5006.

Tornqvist M. 2005. Acrylamide in food: The discovery and its implications: A historical perspective. Adv Exp Med Biol 561:1–19.

Tsuda H, Shimizu CS, Taketomi MK, Hasegawa MM, Hamada A, Kawata KM, Inui N. 1993. Acrylamide; induction of DNA damage, chromosomal aberrations and cell transformation without gene mutations. Mutagen 8:23–29.

Wu YQ, Yu AR, Tang XY, Zhang J, Cui T. 1993. Determination of acrylamide metabolite, mercapturic acid by high performance liquid chromatography. Biomed Environ Sci 6:273–280.

Xiao Y, Tates AD. 1994. Increased frequencies of micronuclei in early spermatids of rats following exposure of young primary spermatocytes to acrylamide. Mutat Res 309:245–253.

Zeiger E, Anderson B, Haworth S, Lawlor T, Mortelmans K, Speck W. 1987. Salmonella mutagenicity tests. III. Results from the testing of 255 chemicals. Environ Mutagen 9(Suppl 9):1–109.

Accepted by—
K. Dearfield

Mutation Research 721 (2011) 21–26

Contents lists available at ScienceDirect

Mutation Research/Genetic Toxicology and Environmental Mutagenesis

journal homepage: www.elsevier.com/locate/gentox
Community address: www.elsevier.com/locate/mutres

Application of the DNA adductome approach to assess the DNA-damaging capability of *in vitro* micronucleus test-positive compounds

Kyoko Kato[a], Eiji Yamamura[a], Masanobu Kawanishi[b], Takashi Yagi[b,*], Tomonari Matsuda[c], Akio Sugiyama[a], Yoshifumi Uno[a]

[a] *Safety Research Laboratories, Mitsubishi Tanabe Pharma Corporation, 1-1-1 Kazusakamatari, Kisarazu, Chiba 292-0818, Japan*
[b] *Environmental Genetics Laboratory, Frontier Science Innovation Center, Osaka Prefecture University, 1-2 Gakuen-cho, Sakai, Osaka 599-8570, Japan*
[c] *Research Center for Environmental Quality Management, Kyoto University, 1-2 Yumihama, Otsu, Shiga 520-0811, Japan*

ARTICLE INFO

Article history:
Received 29 July 2010
Received in revised form 4 November 2010
Accepted 28 November 2010
Available online 23 December 2010

Keywords:
Adductome
DNA adduct
In vitro micronucleus test
LC/MS/MS

ABSTRACT

The *in vitro* micronucleus (MN) test is widely used for screening genotoxic compounds, but it often produces false-positive results. To consider the significance of positive results, it is important to know whether DNA adducts are formed in the cells treated with the test compound. Recently, Matsuda et al. developed the DNA adductome approach to detect DNA adducts comprehensively ([4] Kanaly, et al., Antioxid. Redox Signal., 2006, 8, 993–1001). We applied this method to assess the DNA-damaging capability of *in vitro* MN test-positive compounds. CHL/IU cells were treated with compounds from three categories: (1) carcinogens causing DNA alkylation, ethyl methanesulfonate and *N*-methyl-*N'*-nitro-*N*-nitrosoguanidine; (2) carcinogens producing DNA bulky adducts, 2-amino-6-phenyl-1-methylimidazo[4,5-*b*]pyrene, benzo[*a*]pyrene, 7,12-dimethylbenz[*a*]anthracene, and 4-nitroquinoline-1-oxide, and (3) non-carcinogens, caffeine, maltol, and sodium chloride, with or without metabolic activation. With the conditions in which all test compounds gave positive results in the MN tests, DNA was extracted from the cells and hydrolyzed to deoxyribonucleosides, which were subsequently subjected to LC/ESI-MS/MS analysis. All carcinogens (categories 1 and 2) produced various DNA adduct peaks, and some of the *m/z* peak values corresponded to known adducts. No non-carcinogens produced DNA adducts, indicating that these compounds produced MN through different mechanisms from the adduct formation. These results indicate that the adductome approach is useful to demonstrate DNA damage formation of MN test-positive compounds and to understand their mechanisms of action.
© 2010 Elsevier B.V. All rights reserved.

1. Introduction

In regulatory science, *in vitro* genotoxicity tests are used for examinations of gene mutations and chromosomal alterations due to DNA damage caused by chemicals. The tests can predict carcinogenic potential of new chemicals applicable as pharmaceuticals, industrial materials, food additives, and cosmetic ingredients. If a compound shows a positive result from these tests, further *in vitro* studies to clarify the mechanism of its action (MOA) or *in vivo* genotoxicity tests are required to assess the risk for human health. Kirkland et al. demonstrated recently that the results from *in vitro* genotoxicity tests, especially the chromosome aberration assay and the micronucleus test in Chinese hamster cells and the mouse lymphoma tk locus assay, are highly discrepant from the results from rodent *in vivo* carcinogenicity tests [1].

Direct or indirect DNA reaction with a compound is an example of MOA, and should be first considered after a positive result is obtained in *in vitro* genotoxicity tests [2]. Direct DNA-reactive compounds are considered to have a non-effective threshold in the dose–response relationship in carcinogenesis; however, non-DNA-reactive (indirect) compounds have a threshold. It is considered that there is no cancer risk below the threshold level exposure; therefore, evidence of direct or indirect reaction of the genotoxicity test-positive compound is important for its cancer risk evaluation. A rapid, sensitive, and accurate method to measure cellular DNA damage, that is, direct DNA reactivity in cells, at the same experimental condition as the genotoxicity test will be required to clarify the MOA of the compound.

DNA damage formation can be measured using various analytical methods [3]. The amount of DNA adducts can be determined by measuring radioactive decay or accelerator mass spectrometry of radiolabeled adduct residues in DNA of the cells treated with radiolabeled chemicals. When the labeled compounds are not available, adducts can be measured by ^{32}P post-labeling analysis, physicochemical methods including mass spectrometry, fluorescence

* Corresponding author. Tel.: +81 72 254 9802; fax: +81 72 254 9938.
E-mail address: yagi-t@riast.osakafu-u.ac.jp (T. Yagi).

1383-5718/$ – see front matter © 2010 Elsevier B.V. All rights reserved.
doi:10.1016/j.mrgentox.2010.11.012

spectrometry, and electrochemical detection, or by immunochemical methods. Each of these approaches has different merits and limitations, and the measurement of DNA adduct formation needs a specific experimental protocol that is dependent on the reactivity and characteristics of each compound. None of these methods is very sensitive and accurate to quantitate the amount of DNA damage at the low concentration used in *in vitro* genotoxicity tests.

Recently, Kanaly et al. developed the "DNA adductome" approach to detect DNA adducts comprehensively using high-performance liquid chromatography equipped with tandem mass spectrometry (LC–MS/MS) [4]. The technique allows comprehensive monitoring of multiple types of DNA adducts that have different molecular weights even though their molecular structures are unknown. The technique can detect adducts in cellular DNA with extremely high sensitivity by comparing the "adductome maps" of treated and untreated cells, and is applicable to the analysis of DNA damage produced in various experimental protocols *in vivo* and *in vitro*.

In this study, we combined this adductome approach with the *in vitro* micronucleus (MN) test to examine whether adductome analysis is useful in regulatory science. Chinese hamster lung (CHL) cells were treated with representative MN-inducing compounds with different MOA, and the increase in the MN incidence was confirmed. Following chemical treatment with the identical condition to the MN test, DNA was extracted from the cells, and DNA adducts were measured by adductome analysis. DNA adducts should not be detected in cells treated with non-DNA-reacting compounds such as caffeine, maltol, and sodium chloride, whereas DNA adducts should be detected in cells treated with directly DNA-reacting compounds such as *N*-methyl-*N'*-nitro-*N*-nitrosoguanidine (MNNG) and 4-nitroquinoline-1-oxide (4-NQO). If the adductome analysis in the MN test condition is valid in this pilot study, newly found MN-positive compounds would be rapidly evaluated in terms of whether they are directly or indirectly reactive to DNA by adductome analysis, which may become a new standard method for the MOA evaluation of *in vitro* genotoxic compounds.

2. Materials and methods

2.1. Test chemicals and reagents

Nine compounds were selected for the MN test and adductome analysis, which were classified into three categories: group A, carcinogens known to produce alkyl residues including ethylmethanesulfonate (EMS) and *N*-methyl-*N'*-nitro-*N*-nitrosoguanidine (MNNG); group B, carcinogens known to make bulky DNA adducts including 2-amino-6-phenyl-1-methylimidazo[4,5-b]pyrene (PhIP), benzo[*a*]pyrene (B[*a*]P), 7,12-dimethylbenz[*a*]anthracene (DMBA), and 4-nitroquinoline-1-oxide (4-NQO), and group C, non-carcinogens including caffeine, maltol, and sodium chloride (NaCl). EMS, B[*a*]P, 4-NQO, and caffeine were purchased from Sigma Co. (St. Louis, MO, USA), and the other chemicals were purchased from Wako Chemical (Osaka, Japan). They were dissolved in distilled water (DW), dimethyl sulfoxide (DMSO), phosphate buffered saline (PBS), physiological saline (saline), or minimum essential medium with 10% calf serum (MEM), immediately before treatment (Table 1). The solvent for each test chemical was used as a negative control. If a chemical required metabolic activation to exert its genotoxicity, rat liver S9 mix, which was designed for the *in vitro* chromosomal aberration test (Kikkoman Corporation, Noda, Japan), was added simultaneously during the treatment period (Table 1).

O^6-methyl deoxyguanosine was purchased from Chemsyn Science Laboratories (Kansas, USA). N^7-methyl deoxyguanosine was synthesized according to the method reported by Yang et al. [5]. [$^{15}N_5$, $^{13}C_{10}$]-2-(2′-deoxyguanosine-8yl)-3-aminobenzanthrone ([$^{15}N_5$, $^{13}C_{10}$]-dG-8-ABA) was kindly supplied by Dr. Takamura of Kanagawa Institute of Technology. These compounds were used for chromatogram standards for the LC/ESI-MS/MS analysis.

2.2. Cells

CHL/IU cells were obtained from DS Pharma Biomedical Co. Ltd. (Osaka, Japan) and used in all experiments. The cells were maintained in Eagle's minimum essential medium (MEM; Nissui Pharmaceutical Co. Ltd., Tokyo, Japan) supplemented with 10% heat-inactivated (56 °C for 30 min) calf serum (CS; Hana-Nesco-Bio Co., Tokyo, Japan) in a 5%-CO_2 incubator at 37 °C.

2.3. MN test

The cells were seeded in ϕ60 mm plastic dishes at 1.6×10^4 cells/dish for the micronucleus tests. The cells were treated with the test chemicals for 6 h in the absence or presence of S9 mix followed by a 20-h recovery period (Fig. 1). Then, the cells were trypsinized and counted. Cytotoxicity was evaluated using the relative cell survival rate, which was defined as the number of chemical-treated cells divided by the number of solvent-treated cells. The cells were spun down and then resuspended in KCl hypotonic solution (75 mM) for 5 min at room temperature. The hypotonized cells were fixed twice in methanol:glacial acetic acid (3:1). Finally, the cells were suspended in methanol containing 1% acetic acid and dropped onto glass slides. After drying, the cells were stained with 0.04% acridine orange solution and subjected to microscopic examination. One thousand intact interphase cells were observed using a microscope, and the incidence of the MN cells was calculated. Fisher's exact test was performed for a statistical analysis.

2.4. DNA extraction

The cells were seeded in ϕ150 mm plastic dishes at 10×10^4 cells/dish for DNA extraction. The cells were treated with test chemicals for 6 h in the absence or presence of S9 mix (Fig. 1). The treatment was carried out with the same experimental protocol as the MN test. The cells were detached by trypsinization, and cellular DNA was extracted according to the method described previously [1]. Purified DNA was suspended in distilled water, and the DNA concentration was determined by measuring absorbance at 260 nm using a UV-vis spectrophotometer. An aliquot of DNA (100 μg) was transferred to a 1.5 mL Eppendorf tube and subjected to evaporation.

2.5. Digestion of DNA samples

DNA was enzymatically hydrolyzed to nucleosides by the micrococcal nuclease/spleen phosphodiesterase (MCN/SPD) method or the nuclease P1 method as described below. In the MCN/SPD method, DNA (100 μg) was enzymatically hydrolyzed to 2′-deoxyribonucleoside-3′-monophosphates for 3 h at 37 °C by the addition of 45 μL of buffer (17 mM sodium succinate and 8 mM $CaCl_2$ at pH 6.0) and 9 μL of MCN/SPD mix consisting of 7.5 units/μL MCN (Worthington Biochemical, Lakewood, NJ) and 0.025 units/μL SPD (Sigma, St. Louis, MO). Then, 3 units of alkaline phosphatase, 30 μL of 0.5 M Tris–HCl (pH 8.5), 15 μL of 20 mM $ZnSO_4$, and 200 μL of water were added and further incubated for 3 h at 37 °C.

In the nuclease P1 method, DNA (100 μg) was enzymatically hydrolyzed to 2′-deoxyribonucleoside-5′-monophosphates by the addition of 300 μL of buffer (30 mM sodium acetate at pH 5.3 and 10 mM 2-mercaptoethanol), 15 μL of 20 mM $ZnSO_4$, 15 μL of water, 3 units of alkaline phosphatase (Wako, Osaka, Japan), and 6 units of nuclease P1 (Wako, Osaka, Japan) for 3 h at 37 °C. Then, 60 μL of 0.5 M Tris–HCl (pH 8.5) was added and incubated for another 3 h at 37 °C.

The digested samples were extracted twice with methanol. The resultant methanol fraction was completely evaporated, and the remaining 2′-deoxyribonucleosides were dissolved in 160 μL of 30% DMSO containing an internal standard (11.5 nM [$^{15}N_5$, $^{13}C_{10}$]-dG-8-ABA).

2.6. Adductome analysis by LC/ESI-MS/MS

The analysis was performed using the Shimadzu HPLC System (Shimadzu), which consists of LC-10ADvp bipumps, a SIL-10ADvp autosampler, a Shim-pack XR-ODS (3.0 mm × 75 mm, 2.2 μm, Shimadzu), and a SPD-10 ADvp UV–Vis detector. The HPLC mobile phases A and B were water and methanol, respectively. The HPLC flow rate was set at 0.2 mL/min. The HPLC gradient started at 5% B, was increased linearly to 80% B over 20 min, and returned to the initial condition over 1 min, which was maintained for a further 10 min. The HPLC system was interfaced with a Quattro Ultima Pt (Waters-Micromass) tandem quadrupole mass spectrometer with an electrospray interface. The temperature of the electrospray source was maintained at 130 °C, and the desolvation temperature was maintained at 380 °C. Nitrogen was used as the desolvation gas (700 L/h), and the cone gas was set to 30 L/h. The capillary voltage was set at 3.5 kV. The collision cell pressure and collision energy were set to 3.8×10^{-3} mBar and 15 eV, respectively. The adducts were analyzed by MS/MS using multiple reaction monitoring (MRM). Ion transition was set at $[M+H]^+ \rightarrow [M+H-116]^+$, the [M+H] of which ranged from *m/z* 250 to *m/z* 702. The LC/ESI-MS/MS was set to monitor 32 ion transitions simultaneously in each injection and 10 μL of each sample was injected 15 times. The ion transitions for an internal standard (*m/z* 526 → *m/z* 405) were monitored in each injection. The absorbance at 254 nm was also monitored with a UV–Vis detector to monitor DNA digestion, and the peak area of 2′-deoxyguanosine (dG) was used for data analysis peak normalization as described below.

2.7. Data analysis

DNA adduct peaks were extracted by comparing chromatograms between the controls (solvent-treated samples) and chemical-treated samples using the following criteria: the signal to noise (S/N) ratio of the detected peak should be more than 3, and the peak area should be 3 times larger than the control peak. When a possible adduct peak was detected, a repeated MN test and adductome analysis were

Table 1
Summary of *in vitro* micronucleus tests.

Chemical	Solvent	Dose (μg/mL)	S9 mix	Cytotoxicity (relative cell survival) (%)	MN frequency (%)[b]	Control MN frequency (%)[b]
EMS	PBS	1000	–	101.0	10.15[c]	1.65[c]
MNNG	DMSO	2	–	98.5	13.25[c]	1.90[c]
PhIP	DMSO	12	+	79.5	16.00[c]	0.75[c]
B[*a*]P	DMSO	10	+	52.5	11.00[c]	1.25[c]
DMBA	DMSO	3	+	69.5	17.50[c]	0.75[c]
4-NQO	DMSO	0.5	–	62.1	5.90[c]	0.70[c]
Caffeine	DW	2000	–	92.7	4.35[c]	0.60[c]
Maltol	Saline	200	–	69.3	4.75[c]	0.55[c]
NaCl	MEM[a]	7500	–	85.2	4.00[c]	0.75[c]

[a] Culture medium (MEM supplemented with 10% CS).
[b] Mean of duplicate culture.
[c] $p < 0.001$ vs. controls by Fisher's exact test.

conducted to confirm reproducibility. The peak area was calculated using Masslynx version 4.0 (Waters) and normalized using the peak areas of dG and the internal standard (I.S.) as described by the following equation: Normalized peak area = (peak area of putative DNA adducts)/(dG area)/(I.S. area) × 10^7.

3. Results

3.1. Induction of micronucleated (MN) cells

The results from *in vitro* micronucleus tests with CHL/IU cells are summarized in Table 1. Since all test compounds are known to induce MN cells with various MOA in the presence or absence of S9-mix, the appropriate experimental conditions were determined in the present experiments. All test compounds induced significantly higher MN incidences (>4.0%) than the corresponding controls (solvents) at the concentrations giving higher than 50% cell survival. The incidence of MN cells in the negative control (solvent) ranged from 0.7 to 1.9%. The carcinogens, PhIP, B[*a*]P, and DMBA, significantly induced MN in the presence of S9-mix ($p < 0.001$), whereas other carcinogens, EMS, MNNG, and 4-NQO, and non-carcinogens, caffeine, maltol, and sodium chloride, induced MN in the absence of S9-mix ($p < 0.001$). These treatment conditions were used for the subsequent comprehensive DNA adductome analysis.

3.2. DNA adductome analysis

In the LC–MS/MS chromatograms of all samples derived from the cells treated with the 6 test carcinogens (groups A and B), putative DNA adduct peaks were detected. The detected peak molecular ion (*m/z*), retention times, normalized peak areas, and identified or presumed DNA adducts obtained from the chromatograms are summarized in Table 2. Among the test carcinogens, most adduct peaks were detected by both digestion methods; however, the PhIP-8-dG adduct was detected only by the nuclease P1 method, and the B[*a*]P and DMBA-induced DNA adducts were detected only by the MCN/SPD method. Non-carcinogens(group C) yielded no DNA adduct peaks, even under the conditions that showed positive results in the MN tests. The possible structures of some DNA adducts were estimated from their *m/z* according to the findings of previous reports (Fig. 2).

A representative chromatogram of *N*-methyl-*N*′-nitro-*N*-nitrosoguanidine (MNNG)-treated samples is shown in Fig. S1. Two peaks at *m/z* 282 corresponding to the molecular ion of methylated dG were detected in the MNNG-treated samples. The first peak (retention time: 7.6 min) was identified as N^7-methyl-2′-deoxyguanosine (N^7-methyl-dG), and the second peak (retention time: 13.7 min) was identified as O^6-methyl-2′-deoxyguanosine (O^6-methyl-dG) by comparison with the chromatograms of each standard substance.

For ethylmethanesulfonate (EMS), two peaks at *m/z* 296 were detected (Fig. S2), and the molecular ion corresponded to ethylated dG. The first and second peaks were thought to be N^7-ethyl-2′-deoxyguanosine (N^7-ethyl-dG) and O^6-ethyl-2′deoxyguanosine (O^6-ethyl-dG), respectively, because the amount and polarity of N^7-ethyl-dG would be higher than those of O^6-ethyl-dG [6].

For 2-amino-6-phenyl-1-methylimidazo[4,5-b]pyrene (PhIP), the peaks at *m/z* 450 and 490 were detected (Figs. S3 and S4), and the *m/z* 490 corresponded to *N*-(deoxyguanosin-8-yl)-PhIP (PhIP-8-dG).

For benzo[*a*]pyrene (B[*a*]P), two peaks at *m/z* 570 were detected (Fig. S5). These peaks were considered to be 10-(deoxyguanosine-N^2-yl)-7,8,9-trihydroxy-7,8,9,10-tetrahydrobenzo[*a*]pyrene (B[*a*]P-DE-N^2-dG).

For 7,12-dimethylbenz[*a*]anthracene (DMBA), 12 possible DNA adducts were detected (Figs. S6–S12).

For 4-nitroquinoline-1-oxide (4-NQO), several peaks were detected (Fig. S13–S16). The *m/z* 410 corresponded to 3-(deoxyadenosin-N^6-yl)-4-aminoquinoline 1-oxide (4-AQO-N^6-dA), and *m/z* 426 corresponded to 3-(deoxyguanosine-N^2-yl)-4-aminoquinoline 1-oxide (4-AQO-N^2-dG) and *N*-(deoxyguanosine-8-yl)-4-aminoquinoline 1-oxide (4-AQO-8-dG).

All adduct peaks with their *m/z*, retention times, and peak areas are illustrated in the adductome maps (Fig. 3).

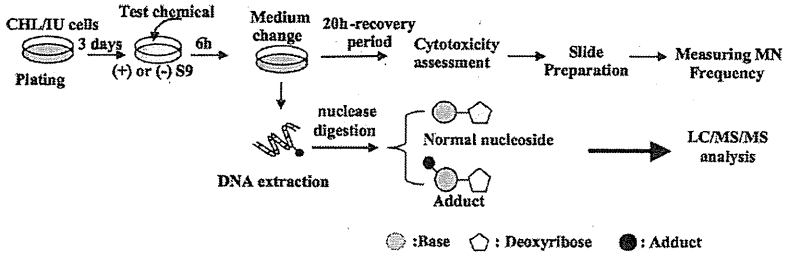

Fig. 1. Schematic outline of the *in vitro* MN test and adductome analysis.

Table 2
Summary of adductome analysis.

Group	Chemical	Peak no.	*m/z*	RT (min)	Normalized peak area		Identified or presumed adducts
					MCN/SPD method	NucleaseP1 method	
A	MNNG	1	282	7.6	2163	2240	N^7-methyl-dG*
		2		13.7	157	158	O^6-methyl-dG*
	EMS	1	296	9.6	2994	5816	N^7-ethyl-dG
		2		16.0	33	235	O^6-ethyl-dG
B	PhIP	1	450	19.1	N.D.	5	–
		2	490	19.6	N.D.	16	PhIP-dG
	B[*a*]P	1	570	22.1	2	N.D.	B[*a*]P-DE-N^2-dG
		2		22.5	6	N.D.	
	DMBA	1	558	24.6	3	N.D.	DMBA-DE-dA
		2	572	19.3	8	N.D.	–
		3		21.4	10	N.D.	–
		4	574	19.3	5	N.D.	DMBA-DE-dG
		5		22S.7	13	N.D.	
		6		23.5	25	N.D.	
		7	590	17.6	12	N.D.	–
		8		18.1	17	N.D.	
		9	596	23.5	5	N.D.	Sodium adducts of No.6
		10	606	18.7	14	N.D.	–
		11		20.7	3	N.D.	–
		12	612	19.3	4	N.D.	–
	4NQO	1	371	14.2	7	4	–
		2	410	12.3	155	112	4-AQO-N^6-dA
		3		17.3	N.D.	6	
		4	426	14.2	4	3	4-AQO-N^2-dG or 4-AQO-8-dG
		5		14.7	4	24	
		6	456	14.6	4	12	–
C	Caffeine Maltol NaCl	No specific peak was detected					

"N.D." means "not detected". "–" represents unknown adduct.
Adducts with and without asterisk show "identified" and "presumed" adducts, respectively.

4. Discussion

In this study, we used the adductome approach to detect the DNA damage caused by the compounds that gave positive results in the MN test condition. Three categories of compounds with different MOA for MN induction were selected. All tested carcinogens were confirmed to form DNA adducts; in contrast, three non-carcinogens yielded no DNA adduct peaks.

In the group A compounds consisting of DNA alkylating agents, O^6- and N^7-methyl-dG and O^6- and N^7-ethyl-dG were detected in the MNNG- and EMS-treated cells, respectively. Although N^3-methyl-dA and N^3-ethyl-dG have been found in other chromatographic analyses [6,7], these adducts were not detected in this adductome analysis, which was probably due to their instability. Another minor lesion, 1-methyl dG, was not detected because its amount was considered to be lower than the detection limit. These results indicate that alkylation of O^6 and N^7 positions of dG would be proof of DNA damage by the group A compounds in the MN-positive experimental condition.

In the group B compounds producing DNA bulky adducts, each compound yielded at least two DNA adduct peaks in the adductome analysis. PhIP yielded two peaks at *m/z* 450 and 490; the former peak is one of unidentified minor adducts [8], but the latter peak is coincident with PhIP-8-dG, the major adduct formed through a reactive intermediate *N*-acetoxy-PhIP [8]. B[*a*]P yielded two peaks at *m/z* 570, which are coincident with the molecular ions of the major adducts B[*a*]P-DE-N^2-dG consisting of four types of stereoisomers [9]. DMBA yielded twelve possible adduct peaks, which agrees with the report showing at least eight DNA adducts induced by DMBA with the ^{32}P-post-labeling analysis [11]. Three DMBA-induced peaks at *m/z* 574 would be stereoisomers of the DMBA-dG adduct, and a peak at *m/z* 558 is coincident with the molecular ion of DMBA-dA, but other peaks are unknown adducts. Six possible DNA adduct peaks were detected in the 4-NQO-treated cellular DNA. Two peaks at *m/z* 410 and 426 correspond to 4-AQO-dG and 4-AQO-dA adducts, respectively, in which several types of 4-NQO binding to C8, N^2, and N^6 of dG and dA are included [12–15], and other peaks cannot be identified because 4-NQO produces various base lesions with different half-life periods [16,17]. These results indicate that the adductome analysis can detect various types of DNA bulky adducts that were identified with the existing methods by other investigators. The efficiency of the adduct peak detection is different between nuclease P1 and MCN/SPD digestion methods in each compound because their enzyme activities on adducted-base excision would vary dependent on the adduct structures. The use of both digestion methods is necessary to detect DNA adducts when new chemicals are tested.

None of the group C compounds, caffeine, maltol, and sodium chloride, which are non-carcinogens but known to produce MN, yielded adduct peaks. Caffeine may interact with DNA repair enzymes and/or nucleotide precursor pools [19], and shows positive results in various genotoxicity tests [18]. Despite a great number of investigations over the past 50 years, the MOA of these compounds is not well understood. The cytotoxic effect of maltol can be explained by its pro-oxidant properties; the maltol/metal complex generates reactive oxygen species (ROS) causing the production of hydroxyl radicals and leading to the formation of DNA base adducts [20]. However, no ROS-related DNA adducts were detected in the present analysis. Sodium chloride increased the incidence of MN cells at extremely high concentrations (c.a. 128 mM). Hyperosmotic medium can cause chromosomal aberrations in CHO cells, mutations at the TK locus in L5178Y mouse lymphoma cells, and at the HPRT locus in V79 cells [21]. However, the mechanisms by which abnormalities are induced in cells subjected to high osmotic pressure are unknown. Although the failure to detect DNA adducts with the non-carcinogens does not mean necessarily that DNA adducts were not formed, DNA adductome is the promising

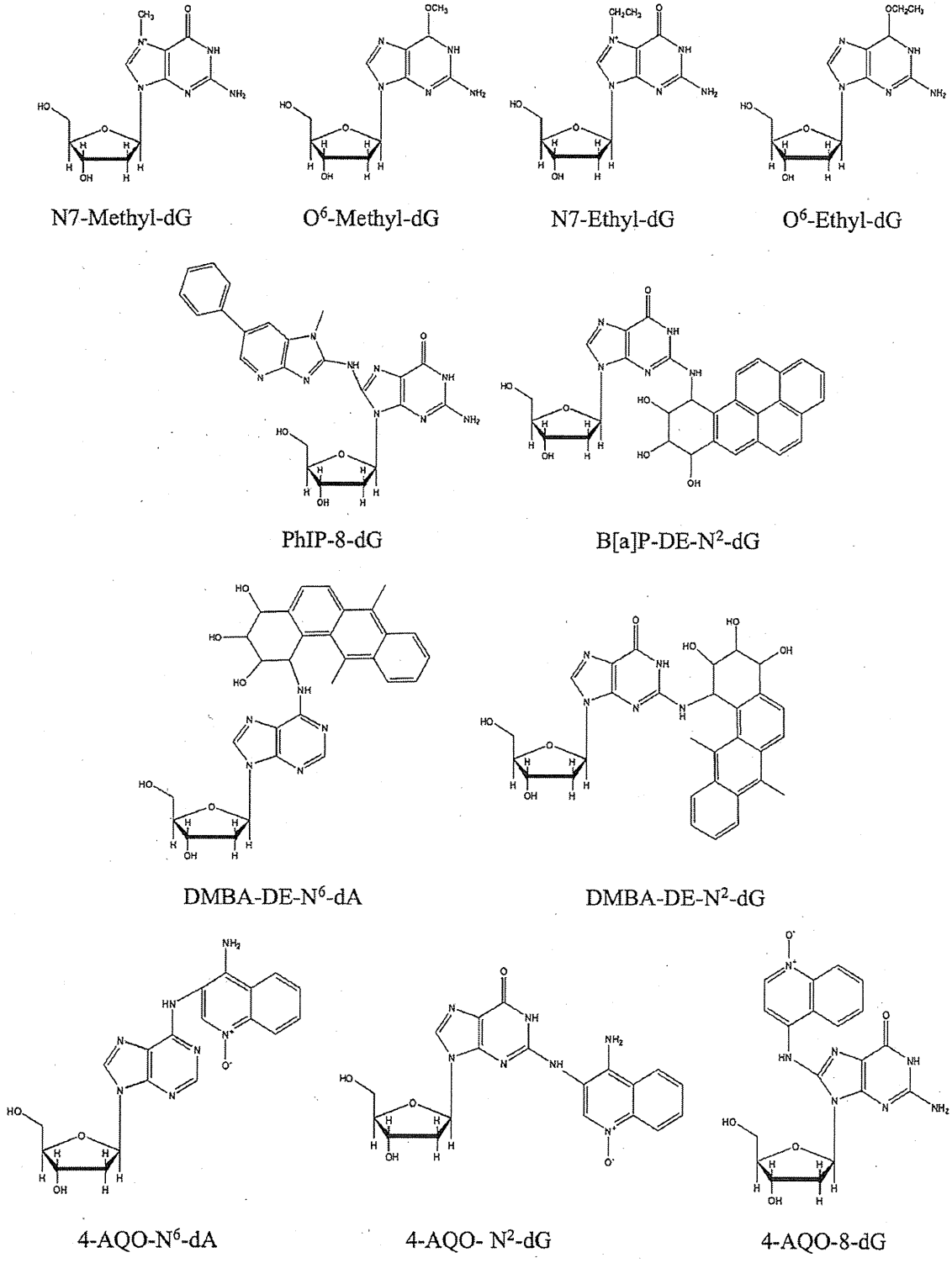

Fig. 2. Structures of DNA adducts estimated from their detected *m/z* values indicated in Table 2. The structures of DMBA-DE-N^6-dG and DMBA-DE-N^2-dG were estimated by the adduction pattern of other PAH compounds.

approach to distinguish false-positive genotoxic compounds from MN-positive compounds. The reliability of this approach will be improved more if the sensitivity of LC/MS/MS equipment is increased and the adductome protocol is more sophisticated.

In summary, with the conditions in which the test compounds significantly increased the frequency of MN cells, only carcinogens (groups A and B) yielded adduct peaks as expected (Table 2 and Fig. 3). The advantages of this adductome approach are as follows: (1) multiple types of DNA adducts can be detected comprehen-